MOLECULAR
PHYSICS

Chlorophyll spectroscopy: conceptual basis, modern high-resolution approaches, and current challenges

Jeffrey R. Reimers[a,b], Margus Rätsep[c], Juha Matti Linnanto[c] and Arvi Freiberg[c,d*]

[a] International Centre for Quantum and Molecular Structures and Department of Physics, Shanghai University, Shanghai 200444, China
[b] School of Mathematical and Physical Sciences, University of Technology Sydney, Ultimo, New South Wales 2007, Australia
[c] Institute of Physics, University of Tartu, W. Ostwaldi 1, 50411 Tartu, Estonia
[d] Estonian Academy of Sciences, Kohtu 6, 10130 Tallinn, Estonia

Abstract. The conceptual formalism to understand the properties and function of chlorophylls in the gas and solution phases as well as in protein matrices is reviewed. This formalism is then applied to interpret modern high-resolution spectroscopic data, resulting from methods such as differential fluorescence line-narrowing spectroscopy and selective fluorescence excitation spectroscopy, which resolve individual vibrational transitions within the inhomogeneously broadened emission and absorption spectra of chlorophyll-a, bacteriochlorophyll-a, and pheophytin-a. Density functional theory and ab initio quantum chemical calculations are applied to interpret this data and fill in missing information needed to understand photosynthetic processes. The focus is placed on recognizing environmental and thermal effects, as well as the roles of Duschinsky rotation and non-adiabatic coupling in controlling the spectra. A critical feature of chlorophyll spectroscopy is determined to be absorption-emission asymmetry. Its ramifications for chlorophyll's function in photosystems are expected to be significant, as most current models for understanding their function assume that absorption and emission are symmetric, i.e. in the absence of relaxation processes, molecules coherently re-emit the light that they absorbed to enact exciton transport. The effect of the Duschinsky rotation is that after vibrational excitation during the electronic transition chlorophylls mostly emit light at different energies to what they absorb, while the effect of non-adiabatic coupling is that the polarization of the light is changed.

Keywords: photosynthetic pigments, selective molecular spectroscopy, absorption-emission asymmetry, density functional theory, non-adiabatic coupling, Duschinsky rotation, Condon and Herzberg–Teller approximations.

1. INTRODUCTION

As the main photosynthetic pigments, chlorophylls and their bacterial counterparts, bacteriochlorophylls, are amongst the most important life supporting molecules on Earth [1]. The distinct role of these molecules lies in their unique optical and redox properties [2,3]. In photosynthetic organisms, such as plants, algae, and bacteria, the pigments facilitate the basic functions of harvesting solar energy as well as the transport of pigment excitations to charge-separation units called *reaction centres*, where the solar energy is converted into chemical energy for both short-term and long-term storage [1–3].

Critical for these functions are not only snapshots of the electronic or nuclear structures of the pigment collections, but also the dynamical transfer of energy between the electronic and nuclear subsystems.

In individual molecules, only local intra-molecular nuclear vibrations are involved in the dissipation of excess energy, delivered as heat following some electronic transition. This excess energy is known as the *reorganization energy* λ and it arises because vertical excitation of a chromophore by light absorption or emission takes more energy than the minimum amount allowed in the final electronic state, with this extra energy then being distributed amongst the nuclear vibrations. In addition, in native photosystems the complex surroundings of each and every pigment chromophore, including other pigments, protein backbone and residues, as well as any solvent, introduce multiple collective nuclear vibrations generally termed *phonons*. These are delocalized to different extents over the photosystem and can be characterized by a quasi-continuum frequency spectrum that typically spans from close to zero to a few hundred wavenumbers in energy. Phonons are instrumental in energy relaxation processes as well as in damping the electronic coherences [4]. In photosynthetic assemblies, the concept of *excitons* acquires significance [5]. The electronic excitation energy remains on a single molecule when the molecule is held in isolation, but in photosynthetic environments it can delocalize over multiple chromophores forming an exciton, again indicating the criticality of the chromophore environment.

Energy dissipation mechanisms related to light absorption and emission also pertain to energy transfer processes from, e.g., an antenna pigment to a reaction centre and also the processes occurring during primary charge separation followed by charge transport reactions. In primitive photosystems such as those in purple bacteria, energy loss may facilitate the system function, as indicated in the energy-funnel model [1,6,7]. The resultant unfortunate consequence, however, is that the dissipated reorganization energy is lost and henceforth not available for functional use. Its minimization is therefore a priority, and more modern photosystems such as cyanobacteria operate by driving electronic processes faster than T_1-type vibrational relaxation can occur [8]. Such electronic processes are treated in Förster excitation-energy transfer theory as occurring by coupled emission of light by one chromophore in an assembly and reabsorption by another, assuming no nuclear relaxation [9]. Understanding of the basic processes of light absorption and emission, and of the intrinsic reorganization energies involved, is therefore critical to the command of all excited-state processes related to solar energy capture.

The role played by phonons is also of major concern, as is the evolution of spectra from the gas phase to isolated molecules in solution and to molecules assembled close together in photosystems. Basically, the electron-phonon interactions dissipate absorbed energy as heat, as do the interactions with intramolecular vibrations. The effect of the phonons on the observed absorption and emission spectra of chlorophylls is barely apparent in low-resolution spectra, but presents a critical aspect pertaining to the interpretation of high-resolution spectroscopic data. This is the phenomenon we will pursue in some detail in this review. Whereas phonons may seem less important from the perspective of the experimental interpretations of molecules in solution (and in proteins) [10,11], their relative importance may be much greater when considering how many times optical energy can get transferred in photosystems before primary charge separation occurs.

In molecular assemblies, the electron-phonon interactions determine both the dynamics and nature of electronic excited states [5,12,13]. Thus, the common Förster excitation energy transfer mechanism emerges when the electron-phonon interactions are strong compared to the electrostatic interaction between the transition dipole densities of neighbouring pigments. The latter coupling as a weak perturbation induces an excitation energy transfer from a localized state of an energy donor to that of an acceptor. In the opposite case of a weak electron-phonon coupling, the zeroth-order electronic states are associated with delocalized excitons that, to a varying extent, embrace a number of pigment molecules. Now, the weak perturbation represented by the electron-phonon coupling results in energy relaxation down to the multiple excitonic states. Extreme cases of strong electron-nuclear coupling (by phonons and/or intramolecular vibrations) result in localization of excitons [12], the process which in solid state physics is called exciton self-trapping [14]. In literature on photosynthesis, strong electron-phonon coupling has been associated with mixing of an optically bright exciton and dark charge transfer states [15,16]. Proper experimental characterization of these states is, therefore, very important in its own right.

Although small molecules in a cold gas phase, such as those produced in a vacuum-expansion supersonic jet, can provide high-resolution spectra for a complete description of the electronic and nuclear structure of

a system, similar quality information for molecules the size of chlorophyll is not yet available [17,18]. Therefore, solid-phase methods including matrix spectroscopy [19] and single-molecule spectroscopy [20,21] are widely applied to facilitate a fundamental understanding of their properties. Yet all condensed-phase systems – doped polymer glasses and pigment-protein complexes among them – suffer from the environment-induced homogeneous and inhomogeneous (or disorder) broadenings. Hence, they are not expected to yield the quality of results that has made gas-phase spectroscopy into such a powerful investigative tool [22].

This paradigm was first broken in the 1970s by the development of frequency-selective laser spectroscopy techniques of fluorescence line-narrowing (FLN) [23] and spectral hole-burning (SHB), independently in Tartu [24] and in Moscow [25]. These breakthrough methods – originally associated with the advancement of studies of prospective laser materials and model chemical systems – were based on the theoretical recognition that the homogenously broadened electronic spectra of guest atoms or ions or molecules fixed at low temperatures in a transparent host matrix can comprise an intense and narrow zero-phonon line (ZPL), an optical analogue of the Mössbauer effect, and a generally broad but sometimes weak phonon sideband (PSB) [22,26,27]. Indeed, Nature often selects molecules, such as chlorophylls, with weak PSBs (i.e., small homogeneous broadening) as they minimize reorganization-energy loss, and hence typically enhance functionality.

The inhomogeneous broadening, being an ensemble effect arising from variations in the local surroundings of guest molecules in the matrix, can be curbed by reducing the size of the ensemble of simultaneously excited or recorded species. In FLN and SHB, this is achieved by resonant excitation by a spectrally narrow laser line of selected ZPLs under the homogeneously broadened absorption band shape. A more sophisticated version of spectrally selective spectroscopy, difference FLN (ΔFLN), combining elements from both FLN and SHB [28,29], was successfully implemented relatively recently [30,31]. This technique provides two important advantages: first, the scattered laser light which otherwise obscures the ZPL in FLN spectra can be effectively eliminated in the difference spectrum, allowing direct measurement of the ZPL; second, the double selection via both SHB and FLN results in the ΔFLN spectrum, which in the low-fluence limit becomes identical to the homogenously broadened spectrum [32], a prerequisite for determination of the electron-phonon coupling from optical spectra of impurity molecules [33].

The great value of the high-resolution solid-state techniques was quickly recognized and now many examples are known from amongst a wide range of fields [19,34–40]. Early application of chlorophyll and other biologically relevant molecules by R. Avarmaa and coworkers from the Institute of Physics of the Estonian Academy of Sciences was an immediate success [41–44]. In all cases, the previously unknown vibrational structure of the fluorescence and the selectively recorded fluorescence-excitation spectra was revealed with unprecedented clarity. Making progress at the most fundamental level, the initial experimental developments of Avarmaa et al. prompted them to introduce a revised assignment of the *Q*-band structure of chlorophyll-a (Chl-a) [26,42], a conundrum actively debated during the next three decades [45–54]. The original spectral measurements remain state-of-the-art to this day, and the conceptual challenges to the then perceived qualitative nature of absorption in Chl-a drove the discussion. Critical issues involved the interpretation of the *x*-polarized intensity as well as the relationship between the high-resolution results and those from low-resolution magnetic circular dichroism (MCD) spectroscopy. Today, line-narrowing spectroscopies continue to be routinely applied to measure high-resolution spectra in photosynthetic pigment-protein complexes. Compared with single-molecule spectroscopy, they achieve supreme signal-to-noise ratios at comparative excitation intensity/fluence attained by implicit ensemble averaging [37,38,55].

This review starts by considering the conceptual framework used to interpret low-resolution and high-resolution data and to perform computational modelling. The basic properties of the electronic spectra of chlorophyll-like molecules (including bacteriochlorophylls, pheophytins, bacteriopheophytins, and porphyrins) were first determined by Gouterman [45,56,57].

In Section 2, we examine the critical aspects of this early model. Basically, two low-energy transitions were predicted, named Q_x and Q_y, along with two high-energy transitions, named B_x and B_y (the "Soret" bands). The labels *x* and *y* depict the primary polarization direction of the transition in the macrocycle pseudo-plane. Primarily, we are concerned with the two low-energy transitions as these dominate most aspects of the light-driven chlorophyll function in photosystems.

Section 3 addresses the varying conceptual bases used to provide qualitative and quantitative descriptions of chlorophyll spectroscopy. It also provides an overview of the computational procedures used in spectral simulations performed based on the results of modern electronic-structure computations. The roles that intramolecular vibrations play in the electronic transitions are varied and complex. Notably, the vocabulary used to describe the interplay of vibrational and electronic factors differ significantly between communities with interests in chlorophyll science, resulting in the expression "electron-vibration coupling" (or equivalently "vibronic coupling") being used with very different meanings. The section integrates these varying terminologies and approaches under a single framework believed to be adequate for the description of all features of chlorophyll spectroscopy of interest. We refer to different vibrations in terms of their ability (1) to distort equilibrium geometries to manifest Huang–Rhys factors [58,59], the quantities that are most widely used in describing both spectra, and (2) to generate non-adiabatic couplings, the quantities that intricately mix the natures of states such as Q_x and Q_y [60–63], as well as the excitonic states localized on different molecules.

A key aspect of Section 3 is the presentation of a basic spectroscopic model, known as the *reflexion approximation*, that perceives absorption and emission spectra as being symmetric. The low-resolution spectra of chlorophylls have long been known to show significant asymmetry. The experimental characterization of this asymmetry, in both low-resolution and high resolution, forms a theme for this review. Sections 2 and 3 together provide the conceptual understanding needed to interpret this asymmetry: (1) The Gouterman model indicates [45] that Q_x and Q_y are very similar in energy, with Q_y identified as the lowest-energy transition and therefore expected to be active in both absorption and emission. On the other hand, the higher-energy transition Q_x is expected to be active only in absorption, generating significant absorption-emission asymmetry. (2) Huang–Rhys factors are generated based on the normal modes of the final state involved in an electronic transition, meaning that they intrinsically differ between absorption and emission as Duschinsky rotation [64] operates to change the form of nuclear vibration in each state. (3) Non-adiabatic couplings can strongly couple Q_x to Q_y to significantly affect spectra, intrinsically introducing asymmetry.

Section 4 avoids the question of the nature and significance of the *x*-polarized intensity of Chl-a by focusing only on the *y*-polarized intensity directly attributable to Q_y. It reviews the high-resolution data obtained by Avarmaa for Chl-a, as well as other modern high-resolution studies for BChl-a and pheophytin-a (Pheo-a) in dilute solution. These are set in the context of associated low-resolution studies. The large asymmetry observed between absorption and emission is interpreted in terms of the effects of Duschinsky rotation, often making the Huang–Rhys factors in absorption and emission very different.

Section 5 proceeds to show how this effect of Duschinsky rotation can be simulated using modern computational methods. This provides basic information by demonstrating how the Duschinsky matrix induces the often-profound observed effects. In current experimental spectra, there is insufficient information to allow direct observation of the critical aspects of the matrix. Hence, this combined experimental-computational strategy is used to provide a complete picture, at a qualitative to semi-quantitative level, of the Q_y absorption and emission processes in chlorophyllides.

Having understood the intrinsic properties of Q_y of Chl-a, Sections 6–8 return to the critical question of the basic qualitative interpretation of its absorption spectrum and its significance for exciton transport in photosystems. Through consideration of non-adiabatic coupling between Q_x and Q_y, all experimental results, including Avarmaa's original provocative high-resolution measurements, can be rationalized. It is not possible to describe the absorption spectrum of Chl-a based on the classical model assuming that dynamics after excitation only occurs on a single potential energy surface. The Q bands of Chl-a can only be understood in relation to a model that treats nuclear vibration and electronic motion on an equal quantum footing, invalidating many normal spectroscopic expectations. We thus show that gas-phase calculations embody most of the features needed for detailed understanding of the effects of solvent on high-resolution spectra, although quantitatively failing in the description of the actual observed properties. More demanding computations that fully solvate the chromophore by explicitly represented (solvent and/or protein) surroundings, combined with inclusion of long-range dielectric properties, will likely be required for further progress.
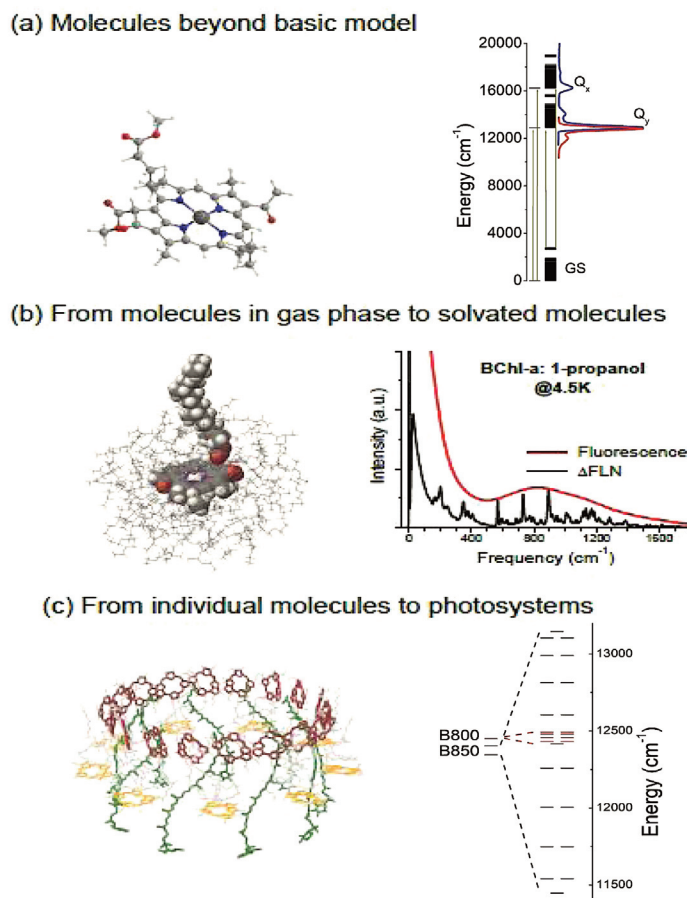
(a) Molecules beyond basic model

(b) From molecules in gas phase to solvated molecules

(c) From individual molecules to photosystems

Fig. 1. Bacteriochlorophyll-a (BChl-a) in different environments: (a) gas phase [66]; (b) solid solution of 1-propanol [67]; (c) LH2 light-harvesting pigment-protein complex from *Rhodoblastus acidophilus* [68]. For simplicity, in the latter structure only pigment molecules are shown: 27 BChl-a (drawn by dark red and yellow colours) and 9 carotenoids (green). See the text for further explanations.

Finding individual pigments in native photosystems is rare. They are usually clumped together, forming tightly bound oligomers and aggregates in protein and solvent surroundings. Elementary electronic excitations in such molecular assemblies are delocalized excitons [5,65]. Some remarkable spectral effects accompanying the assembly of BChl-a molecules into bacterial light-harvesting complexes will be introduced in the final part of this review.

A line of thought followed in this review is sketched in Fig. 1.

2. THE GOUTERMAN MODEL FOR THE VISIBLE ABSORPTION SPECTRA OF PORPHYRINS AND CHLOROPHYLLIDES

The basic model for the interpretation of the visible spectroscopy of porphyrins and chlorophyllides was developed by Gouterman in the early 1960s [45,56,57]. It is highly analogous to the model used to describe benzene and expanded-ring molecules that was featured in the first-ever "ab initio" calculation [69], for which graphene appears as the 2D asymptotic limit. The key elements of the visible spectroscopy are taken to be dominated by four frontier orbitals, as illustrated in Fig. 2.

For benzene, these are a doubly degenerate highest-occupied molecular orbital (HOMO) and a doubly degenerate lowest-unoccupied molecular orbital (LUMO). In a metal porphyrin of D_{4h} symmetry such as
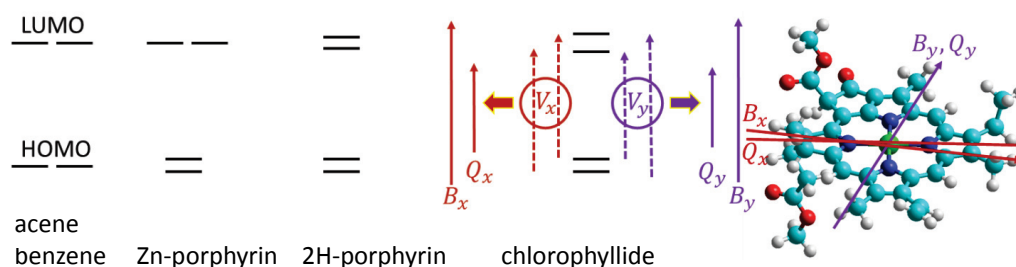
Fig. 2. Basic Gouterman model for the spectroscopy of porphyrins and chlorophylls and its relationship to benzene and the acenes. Increasing degrees of asymmetry split the doubly degenerate HOMO and LUMO orbitals of benzene, with the visible-region spectroscopic transitions Q_y, Q_x, B_y, and B_x (solid arrows) arising after strong configuration interactions V_x and V_y between pairs of the embodied single-electron transitions (dashed arrows). The directions of the associated (approximately in plane) transition dipole moments calculated by CAM-B3LYP are indicated in the molecular model for methyl-chlorophyllide-a: C – cyan, H – white, N – blue, O – red, Mg – green.

zinc porphyrin, the LUMO remains doubly degenerate, but the HOMO splits in energy by a small amount. In a free-base (2H) porphyrin analogous to pheophytins, the LUMO also splits. In chlorophyll-like molecules, the low symmetry inherently breaks all degeneracies, with the LUMO usually splitting the most. For all of these compounds, four single-electron excitations can be constructed from amongst the four key orbitals, as shown in the figure. In the high-symmetry acenes and porphyrins, these four excitations split into pairs of different symmetry labelled x and y, with strong configuration interactions V_x and V_y occurring within each pair. As a result, the four one-electron transitions expected with similar energies split into pairs that are well-separated from each other in energy owing to the configuration interaction. This situation has some analogy with energy transfer between chromophores as the Förster and Dexter mechanisms for exciton coupling are merely different aspects of electron correlation; in the case of a single chlorophyll, the two strongly coupled transitions exist spatially overlapped on the one and the same molecule.

The labels x and y pertain to polarization directions within the macrocycle plane, as depicted in Fig. 2. They are naively expected to be orthogonally polarized, but in reality, the angle between them varies to some degree. With regard to Q_y and Q_x, the observed angle between them is ca 20° from the right angle and is reported as being either 70° [48,70] or 110° [71,72], with studies focusing on their differentiation [73] concluded that it is 70°. The polarization directions depicted in the figure are from CAM–B3LYP calculations, which predict 67°.

The configuration interaction causes the lower-energy component excitations, labelled Q, to be weak compared to the high-energy components, labelled B. This effect is reduced in chlorophyll-like molecules compared to that in benzene and porphyrins, especially for the y bands, owing to the significant HOMO and LUMO splitting and the reduction in V_y. As a result, Q_y is intense. Nevertheless, the basic pattern is maintained in x symmetry and so the inherently forbidden nature of Q_x persists.

Beyond the Gouterman model, many other transitions in chlorophylls have been anticipated, and the observed spectra in the Soret region and beyond clearly show the effects of other excitations. For example, the N bands are charge-transfer bands with solvent-sensitive energies close to the energies of the Soret bands. Due to their charge-transfer nature, their accurate modelling poses significant challenges to computational methods [53,54,74,75]. Such issues are critical when considering the MCD spectra and other properties of the Soret bands, but are not the subject of this review. Historically, DFT-based proposals [53,54] were made that placed non-Gouterman transitions overlapping with the Q bands, but modern spectral assignments can accommodate all observed spectral features in this region without such complication [63].

3. CONCEPTUAL FORMALISM TO PROVIDE UNDERSTANDING FOR THE SPECTROSCOPY OF CHLOROPHYLLS AND THEIR APPLICATION TO FIRST-PRINCIPLES COMPUTATIONAL SPECTRAL MODELLING

Spectroscopy provides measurements on systems containing electrons and nuclei that in reality are quantum particles which interact in very complex ways. To make progress in both conceptual understanding and computational modelling, this complexity needs to be simplified by the introduction of models. Different models are possible, with each capturing a good description of some basic aspects, whilst neglecting others. The ignored aspects appear as *couplings* that connect together the basic physical quantities featured. How easy a basic model is to solve, how descriptive of key experimental observables its parameters are, and how easy it is to obtain the full quantum solution numerically from its provided starting point, determine the usefulness of each model for conceptualization and for computation. Over the years, a wide variety of models have been used to describe the spectroscopic properties of chlorophylls, leading to different notations and computational implementations. We start by providing an integrated framework in which these models and their notations can be discussed, while showing how they lead to basic understanding of chlorophyll spectroscopy and function.

Most models used apply some type of adiabatic separation of the wavefunctions of electrons and nuclei. In addition, the separation of the wavefunction into contributions from intermolecular and intramolecular contributions is an essential element in the consideration of condensed-phase spectroscopy. We follow essentially the spectroscopic formalism unified by Sponer and Teller [76] in 1941, with a small enhancement, also showing how modern practices relate.

3.1. Treatment of intramolecular and intermolecular nuclear motions

Intramolecular motions are most commonly treated as discrete entities, constructing Hamiltonians that explicitly describe their influences. When considering the properties of molecules in condensed phases, these motions are typically labelled as *vibrations*. Alternatively, intermolecular motions are infinite in dimensionality and thus are difficult to treat by explicit representation. Hence, they are depicted usually in terms of their collective effect and are labelled as *phonons*.

To focus on collective effects, wavefunctions for phonons and wavefunctions for electrons are usually treated by a model in which the phonons are perceived as non-interacting with both the vibrations and the electrons. Such a model is broadly termed a *crude adiabatic* model [61,62,77–79]. From its standpoint, all dependences of electronic properties on the properties of the phonons are deemed to arise from what is then appropriately described as *electron-phonon* coupling [22,26,65,80–83]. Specifying this coupling as being linear in the phonon position coordinate leads to analytical expressions pertinent to high temperatures that form the basis of our understanding of how environments modulate molecular spectroscopy and reactivity [81,83]. Alternatively, crude adiabatic models that treat molecules in an assembly as independent units may be proposed, allowing (intermolecular) electronic couplings and exciton couplings to be defined [9,65,83,84].

3.2. Using the Born–Oppenheimer approximation to separate vibrational and electronic properties

All spectroscopic models introduce a zeroth-order Hamiltonian by neglecting selected terms, which is then solved exactly, with the neglected terms reintroduced then as couplings. Crude adiabatic models, such as those indicated above applied to treating phonons, treat the nuclear-position dependence of the electronic wavefunction as couplings. This approach is typically sufficient for the consideration of the properties of simple materials, facilitating the widespread application of crude adiabatic models in this context, but this position dependence becomes a critical defining aspect when considering the spectroscopy and reactivity of molecules. The explicit inclusion of the nuclear position at zeroth order in the model Hamiltonian allows for many molecular properties to be treated analytically.

An alternative adiabatic approach to the crude adiabatic model for separating the effects of vibrations and electrons is the Born–Oppenheimer (BO) approximation [58,79]. In this, all couplings involving the nuclear vibrational position operator are eliminated from the zeroth-order Hamiltonian. This description forms the basis of understanding spectroscopy and reactivity throughout Chemistry and Biochemistry, having also dominated the early years of research in Physics [76] and often incorrectly described as "exact" [80] owing to its perceived generality.

Within the BO approximation, systems are treated as having *uncoupled* electronic and nuclear motions occurring on classical-like potential energy surfaces. Such surfaces may be predicted by electronic-structure calculations as well as inferred from experimental data. Low-resolution spectroscopies reveal gross properties such as the average energy of a final electronic state at the geometry of the initial state, and how much energy is released as heat during the ensuing nuclear relaxation. High-resolution spectroscopies reveal much more information concerning the nature of the vibrational motions in the final state, and possibly the initial state as well. In both cases, experimental data requires a conceptual model for its interpretation, the application of which reveals fundamentally important information.

The description of the photophysical processes occurring on a single molecule, as viewed within the BO approximation and applied to the Q-band spectra of chlorophyll-like molecules, is sketched in Fig. 3. This description can include bond dissociation and rearrangement in its zeroth level [76], but this feature is not required in order to understand the spectroscopic properties of chlorophylls, and so much simpler BO potential energy surfaces are caricatured in the figure for the ground state (S_0), as well as for Q_x and Q_y. Electronic potential energy, as determined, e.g., from some electronic structure computational procedure or inferred from experiment, is plotted on the vertical axis, against some generic nuclear position coordinate depicted on the horizontal axis. There are $3n$-6 such nuclear coordinates k for a polyatomic molecule with n atoms, and hence this surface is, in reality, very highly dimensional in nature. Nevertheless, the depiction of a single nuclear position coordinate is sufficient for our needs. Marked by horizontal lines on each BO potential energy surface are characteristic vibrational energy levels. These levels include contributions from all molecular vibrational modes, with the lowest energy level labelled "0", depicting zero-point vibrational motion in each mode. Vibrational levels marked "1" depict the set of $3n$-6 levels obtainable by adding one
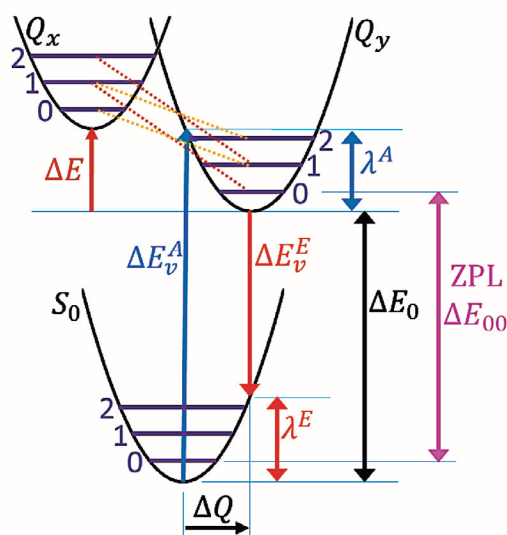

Fig. 3. Critical aspects pertaining to the Q-band spectra of chlorophylls sketched on potential energy surfaces (energy versus a generalized geometrical variable). Vibrational levels corresponding to 0, 1, and 2 vibrations present in only one of the many normal modes of vibration of each state are shown. Emphasized are labels descriptive of Q_y spectroscopy: the geometry difference between the adiabatic state minima ΔQ; the vertical absorption and emission energies, ΔE_v^A and ΔE_v^E, respectively; the associated reorganization energies λ^A and λ^E; the adiabatic transition energy ΔE_0; and the energy of the ZPL origin ΔE_{00}. Marked is also the adiabatic energy gap of Q_x from Q_y ΔE, and the non-adiabatic couplings indicated by dashed lines that link specific vibrational levels of Q_x and Q_y.

quantum of energy to only one of the vibrational modes; these lines are known as *vibrational fundamentals*. Indicated are also levels marked "2" that involve the distribution of two quanta into the vibrational modes, providing examples of *vibrational overtones*.

An important quantity is the adiabatic energy difference between the minima of the BO surfaces. These are labelled ΔE_0 (energy of Q_y above S_0) and ΔE (energy of Q_x above Q_y) in Fig. 3. These quantities are easy to determine computationally, but difficult to determine experimentally, as this would require detailed understanding of all vibrational properties of the two electronic states involved. From experiments, the analogous quantity ΔE_{00} is easier to determine as it is the energy required to transfer a minimally vibrating molecule in its initial electronic state to a minimally vibrating molecule in its final electronic state. A line in a spectrum assigned to this process is called the ZPL; another notation for this line is the 0-0 *band origin*. Such a measurement presumes that high-resolution spectroscopic data is available, but alternatively, its value can often be reliably determined by fitting low-resolution band contours.

Other critical quantities required to understand molecular spectra are the vertical transition energies ΔE_v^A for absorption and ΔE_v^A for emission that are labelled in Fig. 3, as well as their associated reorganization energies λ^A and λ^E. The vertical transition energies are easy to calculate as all one needs to do is determine the energy of the final electronic state at the equilibrium geometry of the initial electronic state. Often these reorganization energies are easy to estimate from observed data as the vertical transition energies are well approximated by the maximum of a broad band and, in general (as is more appropriate for chlorophylls), from integrals over either low-resolution or high-resolution spectra:

$$\lambda^A = h \frac{\int_0^\infty A(v)dv}{\int_0^\infty A(v)/v\,dv} - hv_{00}, \quad \lambda^E = hv_{00} - h\frac{\int_0^\infty E(v)/v^2\,dv}{\int_0^\infty E(v)/v^3\,dv}, \tag{1}$$

where $v_{00} = \Delta E_{00}/h$, $A(v)$ is the observed absorption as a function of frequency v, and $E(v)$ denotes the observed emission when the scan is performed linear in frequency; if emission is scanned linear in wavelength as $E(\lambda)$, then the conversion $E(v) = E(\lambda)/v^2$ must first be applied. The reorganization energies provide the most meaningful descriptions of the bandwidth of an electronic transition, specifying the amount of energy that, on average, is lost as heat as a result of the optical process. Such quantities are critical to the understanding of light absorption, emission, and energy transport in photosystems.

Next, we consider the nature of the position coordinate sketched on the horizontal axis in Fig. 3. Position space may be described using the vector $\mathbf{x}$ containing the $3n$ Cartesian coordinates of the atoms in the molecule. More informative representations can be constructed in terms of the $3n$-6 independent normal modes of vibration of some particular electronic state, expressed generally as

$$\mathbf{Q} = \mathbf{Q}_{zpt}^{-1}\mathbf{CM}^{1/2}\mathbf{x}, \tag{2}$$

where $\mathbf{M}$ is a diagonal matrix specifying the atomic mass associated with each Cartesian coordinate, $\mathbf{C}$ represents the (orthogonal) normal-mode matrix that specifies the directions in which each atom moves during each vibration, and $\mathbf{Q}_{zpt}$ is the diagonal matrix containing the zero-point motional extent, i.e., $\mathbf{Q}_{zpt,k} = \left(\frac{2\pi v_k}{\hbar}\right)^{1/2}$ denotes the value of the displacement of mode k when the increase in energy is $hv_k/2$ and the vibrational frequency is v_k. Vibrational frequencies and normal-mode matrices can be readily determined for the three chlorophyll electronic states of interest using modern computational software. Important is the minimum-energy geometries of an electronic state, expressible as

$$\mathbf{Q}_0 = \mathbf{Q}_{zpt}^{-1}\mathbf{CM}^{1/2}\mathbf{x}_0, \tag{3}$$

where x_0 is the equilibrium geometry in Cartesian coordinates. Explicitly marked in Fig. 3 is the displacement vector $\Delta\mathbf{Q}$ that depicts the change in geometry between the S_0 and Q_y states. This notation is simplistic, however, as such vectors can be defined in terms of the normal coordinates of *either* of the states involved.

The most useful definition is provided via the normal coordinates of the final state, producing vectors directly pertinent to absorption and emission spectra, e.g., for Q_y:

$$\Delta \mathbf{Q}^A = \mathbf{Q}_{Qy,zpt}^{-1} \mathbf{C}_{Qy} \mathbf{M}^{1/2} \Delta \mathbf{x} \quad \text{and} \quad \Delta \mathbf{Q}^E = -\mathbf{Q}_{S0,zpt}^{-1} \mathbf{C}_{S0} \mathbf{M}^{1/2} \Delta \mathbf{x}, \tag{4}$$

respectively, where $\Delta \mathbf{x}$ is the change in the Cartesian coordinates from S_0 to Q_y.

3.3. Mathematical form of the basic Born–Oppenheimer approximation and additional approximations often used to interpret and simulate spectroscopy

Mathematically, the result of the application of the BO approximation (further named as Approx. 1) is that the electron-vibration Hamiltonian pertinent to Q-band spectroscopy can be written as

$$\mathbf{H} = \begin{bmatrix} V_{S0}(\mathbf{Q}) + T(\frac{\partial^2}{\partial \mathbf{Q}^2}) & 0 & 0 \\ 0 & V_{Qy}(\mathbf{Q}) + T(\frac{\partial^2}{\partial \mathbf{Q}^2}) & 0 \\ 0 & 0 & V_{Qx}(\mathbf{Q}) + T(\frac{\partial^2}{\partial \mathbf{Q}^2}) \end{bmatrix}, \tag{5}$$

where $V_{S0}(\mathbf{Q})$, $V_{Qy}(\mathbf{Q})$, and $V_{Qx}(\mathbf{Q})$ are the BO potential energy surfaces of each state and T is the nuclear kinetic-energy operator. From a computational perspective, electronic-structure programs are usually applied to evaluate as much as is needed for each potential energy surface. Then the full separation of electronic and nuclear motions inherent in the BO approximation allows for the determination of the vibrational energy levels $E_{S0,\mathbf{m}}$, $E_{Qy,\mathbf{m}}$, and $E_{Qx,\mathbf{m}}$ and associated vibrational wavefunctions $|\chi_{S0,\mathbf{m}}\rangle$, $|\chi_{Qy,\mathbf{m}}\rangle$, and $|\chi_{Qx,\mathbf{m}}\rangle$ for each electronic state individually, where $\mathbf{m}$ is a vector listing the number of vibrations excited in each of the $3n$-6 vibrational modes of the molecule.

To predict spectra, the analogous electronic dipole-moment operator $\boldsymbol{\mu}$ is required, a quantity that can also be readily evaluated by electronic-structure programs. As the BO approximation eliminates all couplings between states, only the diagonal matrix elements of $\boldsymbol{\mu}$ are required to calculate rotational and vibrational spectra, whereas merely the appropriate off-diagonal matrix element is required for electronic spectra, known as the *transition-dipole matrix element*. At 0 K, only transitions from the zero-point level of the initial state are allowed, with vibrational line intensities within an electronic spectrum given by the vibrational integrals

$$\frac{A_{\mathbf{m}}}{\nu} = \frac{E_{\mathbf{m}}}{\nu^3} = \left\langle \chi_{i,0} | \mu_{if}(\mathbf{Q}) | \chi_{f,\mathbf{m}} \right\rangle^2, \tag{6}$$

where i is the initial electronic state and f the final electronic state. At finite temperature, additional lines arising from Boltzmann-weighted higher vibrational levels of the initial electronic state must also be evaluated.

Whereas the procedure needed to simulate electronic spectra appears straightforward, numerical difficulties arise as the effort in determining the vibrational energy levels and wavefunctions increases exponentially with the number of vibrational modes included and the maximum number of quanta allowed in each vibration. To proceed, approximations are usually introduced that limit the complexity of the BO potential energy surfaces and transition-moment profiles. This situation is also very pertinent to the extraction of basic system properties from experimental data, and analogous approximations are usually introduced during data fitting, which facilitates the ready comparison of results. Some of the common additional approximations are as follows:

Approx. 2: The harmonic approximation. Each BO potential energy surface is (independently) approximated by a quadratic function, e.g.,

$$V_{S0}(\mathbf{Q}) = \frac{1}{2} \sum_k \frac{h\nu_{S0,k}}{2} \left(Q_{S0,k} - Q_{S0,k,0} \right)^2 \quad \text{and} \quad V_{Qy}(\mathbf{Q}) = \Delta E_0 + \frac{1}{2} \sum_k \frac{h\nu_{Qy,k}}{2} \left(Q_{Qy,k} - Q_{Qy,k,0} \right)^2. \tag{7}$$

Using analytical second-derivative code, all parameters in these equations are readily evaluated by modern electronic-structure software. Note, however, that the vibration frequencies and normal modes of each state are different, meaning that more parameters are involved in these equations than are decipherable from observed high-resolution spectra for molecules the size of chlorophylls. Moreover, the degree of difficulty of evaluating the integrals in Eq. (6) for such general harmonic potentials increases exponentially with size so that this process is often not feasible. Hence, more restrictive approximations are often introduced in order to make progress in understanding chlorophyll spectroscopy.

Approx. 3: Neglect of Duschinsky rotation. The relationship between the normal modes of the initial and final states is specified by the Duschinsky rotation matrix

$$\mathbf{D} = (\mathbf{C}_i)^T \mathbf{C}_f. \tag{8}$$

The Duschinsky matrix is a rotation matrix with $3n$-7 independent degrees of freedom, and its neglect significantly reduces the number of parameters in any spectroscopic model used to interpret experimental data. It also provides a simple scheme for the determination of the integrals in Eq. (6) as these can now be written as products of one-dimensional integrals evaluated for each vibrational mode. With the use of the Duschinsky rotation matrix, the displacement vectors for absorption and emission can be related to each other as

$$\Delta Q_l^A = - \sum_{k=1}^{3n-6} \left(\frac{\nu_{Qy,l}}{\nu_{So,k}} \right)^{1/2} D_{kl} \, \Delta Q_k^E. \tag{9}$$

Approx. 4: Neglect of frequency variation, i.e., setting $\nu_{i,k} = \nu_{f,k}$ for all k. This effect is minor in comparison to the neglect of Duschinsky rotation in terms of its spectral effects, but also significantly decreases the number of parameters used in models to describe spectra.

Approx. 5: Neglect of the geometrical dependence of the transition moment operator – the *Condon approximation*. This approximation simply sets $\bar{\mu}_{if}(\mathbf{Q})$ to a constant value. The resulting integrals in Eq. (6) are then termed *Franck–Condon factors*.

Approx. 5a: A related alternate approximation to the Condon approximation is the Herzberg–Teller approximation that is particularly pertinent if an electronic transition is forbidden at the equilibrium geometry of the initial state, but becomes allowed owing to zero-point vibration beyond this geometry. The transition moment vector function is then taken to be linearly proportional to displacement

$$\bar{\mu}_{if}(\mathbf{Q}) = \sum_{k=1}^{3n-6} \bar{\mu}_{if,k} \Delta Q_{f,k}. \tag{10}$$

By selecting combinations of approximations 1–5, different models for interpreting experimental data and computational spectral simulations can be devised.

A common approach applied to the spectroscopy of chlorophyll-like molecules is to use Approx. 1 (the BO approximation), Approx. 2 (the harmonic approximation), Approx. 4 (the equal frequency approximation) and Approx. 5 (the Condon approximation). Indeed, this is the approach used to interpret most low-resolution and high-resolution spectra considered in this review; note specifically that Duschinsky rotation is not neglected (see Approx. 3). This set of approximations facilitates analytical evaluation of the Franck–Condon factors, allowing the relative intensities of the vibrational lines in a spectrum to be expressed in terms of *Huang–Rhys factors* [58] for each vibrational mode

$$S_k^A = \frac{\left(Q_k^A \right)^2}{2} \quad \text{and} \quad S_k^E = \frac{\left(\Delta Q_k^E \right)^2}{2} \tag{11}$$

as

$$\frac{A_m}{A_{00}} = \left(\frac{\nu_m}{\nu_0} \right) \prod_k \frac{\left(S_k^A \right)^{m_k}}{m_k!} \quad \text{and} \quad \frac{E_m}{E_{00}} = \left(\frac{\nu_m}{\nu_0} \right)^3 \prod_k \frac{\left(S_k^E \right)^{m_k}}{m_k!} \tag{12}$$

in absorption and emission, respectively.

A feature useful in experimental data interpretation is that if a high-resolution 0–1 line is clearly resolved from its background, then the Huang-Rhys factor, and hence the magnitude of the geometrical displacement, can be read off the observed intensity ratio as, e.g.,

$$\frac{A_1}{A_{00}} = \left(\frac{\nu}{\nu_0}\right) S^A. \tag{13}$$

Unfortunately, rarely are lines so isolated in the spectra of large molecules such as chlorophylls, and hence experimental data interpretation usually proceeds by fitting the complete observed spectrum to the general form given in Eq. (12). This can be performed efficiently as the products in the general expression above can be evaluated in a linear-scaling fashion by spectral convolution techniques.

The Huang–Rhys factors have other important uses. Their sum

$$S = \sum_k S_k \tag{14}$$

represents the total number of vibrational quanta that are excited at 0 K as a result of an electronic transition. The energy dissipated by each mode, and the total reorganization energy, can also be expressed in relation to them:

$$\lambda_k = h\nu_k S_k \text{ and } \lambda = \sum_k \lambda_k. \tag{15}$$

3.4. The reflexional approximation and anticipated absorption-emission spectral symmetry

In the above conceptualization of electronic spectroscopy, quite different absorption and emission spectra are expected as the Huang–Rhys factors for each S^A and S^E differ, leading to different total reorganization energies λ^A and λ^E, respectively. This difference is caused by the effect of the Duschinsky matrix, changing the form of the normal modes in the initial and final states. If this effect is neglected, i.e., $\mathbf{D} = \mathbf{1}$, then $S_k^E = S_k^A$. If the vibration frequencies in each state are also the same, then absorption and emission spectra will appear as mirror images of each other, reflected about the ZPL. This is known as the *reflexion* approximation and can be derived semi-classically by projecting the initial-state vibrational zero-point wavefunction onto the final state, binning the new energy distribution thus obtained.

It has been widely anticipated that the reflexion approximation should hold, as changes to force constants induced by electronic transitions can be small, particularly in large molecules. This approximation has been extensively used in considering the transport of energy between chromophores in a photosystem: basically, it means that if a chromophore absorbs a photon and re-emits it before nuclear relaxation can induce dephasing or release the reorganization energy, then the photon will be coherently re-emitted.

The same set of approximations discussed previously in the context of conceptual descriptors for observed spectra can also be applied to the prediction of spectra based on computed BO potential energy surfaces and transition moment profiles, revealing features that directly correspond to the applied experimental interpretation. If needed, the approximation of equal frequencies in the initial and final states can be lifted, using in the first approximation the average initial-state frequency as specified by the Duschinsky-matrix elements for each final-state mode [85]. In addition, full simulations without approximating the ground-state frequency are possible and provided for in commercial software such as Gaussian-16 [86].

3.5. Breakdown of the BO approximation: non-adiabatic coupling

The BO approximation eliminates all coupling between nuclear position and electronic motion, but neglects residual influences of the nuclear momenta on the electronic motion. Without approximation, the full-quantum Hamiltonian pertinent to the Q-band spectra of chlorophyll-like (isolated) molecules can be expressed in terms of the BO adiabatic potential energy surfaces $V_{S0}(\mathbf{Q})$, $V_{Qy}(\mathbf{Q})$, and $V_{Qx}(\mathbf{Q})$ as

$$\mathbf{H}^{\text{exact}} = \begin{bmatrix} V_{S0}(\mathbf{Q}) + T\left(\frac{\partial^2}{\partial \mathbf{Q}^2}\right) + DC_{S0} & FD_{S0,Qy}\frac{\partial}{\partial \mathbf{Q}} + SD_{S0,Qy} & FD_{S0,Qx}\frac{\partial}{\partial \mathbf{Q}} + SD_{S0,Qx} \\ FD_{S0,Qy}\frac{\partial}{\partial \mathbf{Q}} + SD_{S0,Qy} & V_{Qy}(\mathbf{Q}) + T\left(\frac{\partial^2}{\partial \mathbf{Q}^2}\right) + DC_{Qy} & FD_{Qy,Qx}\frac{\partial}{\partial \mathbf{Q}} + SD_{Qy,Qx} \\ FD_{S0,Qx}\frac{\partial}{\partial \mathbf{Q}} + SD_{S0,Qx} & FD_{Qy,Qx}\frac{\partial}{\partial \mathbf{Q}} + SD_{Qy,Qx} & V_{Qx}(\mathbf{Q}) + T\left(\frac{\partial^2}{\partial \mathbf{Q}^2}\right) + DC_{Qx} \end{bmatrix}, \quad (16)$$

where the diagonal corrections *DC* represent mass-dependent contributions to the adiabatic potential energy surfaces, *FD* are first-derivative (momentum) non-adiabatic couplings, and *SD* are second-derivative (kinetic-energy) non-adiabatic couplings. The non-adiabatic couplings interconnect the electronic states as a function of the vibrational momentum and kinetic energy. In the absence of non-adiabatic couplings, spectroscopy can be described semi-classically in terms of dynamics occurring on the three isolated classical-like potential energy surfaces. The reflexional approximation follows simply from the classical dynamics expected on such surfaces and is not an intrinsic quantum phenomenon. When non-adiabatic couplings are allowed, no such classical interpretation is possible. Electronic and nuclear wavefunctions become tightly coupled, and only the full solution of the quantum equations can predict realistic spectra. Similarly, any model used to interpret experimental spectra must consider the full quantum nature of the coupled electrons and nuclei.

Modelling of non-adiabatic effects can be achieved by direct solution to Eq. (16), calculating the *DC*, *FD*, and *SD* contributions using electronic-structure methodologies. However, only the *FD* contribution is widely available in modern codes. The idea that this term should dominate is a naïve expectation based on the observation that it is a linear coupling whereas *DC* and *SD* involve quadratic couplings, with couplings usually taken to be small. Contrary to this expectation, these terms appear together in the BO description of the exact Hamiltonian owing to the *cusp catastrophe* that pertains to potential energy surfaces as they intersect at conical intersections. The dynamics of systems around any cusp is chaotic [87], meaning that very large basis sets are required to achieve numerical convergence and that truncated power expansions, such as inclusion of only the first-derivative correction, are likely to produce very poor results [88,89].

In the original work of Born and Oppenheimer [90], the full electron-vibration Hamiltonian was taken and expanded in a power series of the ratio of quarter power of the electron and nuclear masses. They showed that as this ratio goes to zero, then the terms identified as *DC*, *FD*, and *SD* in Eq. (16) will also all go to zero. No successful numerical strategy for emulating their derivation in quantitative calculations is known, however, with current computational approaches evaluating these terms directly rather than through a mass-ratio expansion. Indeed, it became known in the 1950s through the development of adiabatic electron-transfer theory [91–93] that non-adiabatic processes were in fact controlled by much more complex (mass-dependent) effects. More generally, the mass-ratio expansion fails to be useful at conical intersections, the regions of greatest interest [94]. If the geometry of S_0 is sufficiently removed from the $Q_x - Q_y$ conical intersection for the interaction to be treated in terms of a single antisymmetric vibration of frequency ν and reorganization energy λ interacting with an exciton-coupled $Q_x - Q_y$ pair with coupling strength J, then the BO approximation will be valid whenever [89]

$$\frac{1}{8Q_c^2} = \frac{\lambda h \nu}{16J^2} \ll 1, \quad (17)$$

where the displacement Q_c is known as the *cusp radius* that specifies the range through which *DC*, *FD*, and *SD* exert influence around the diabatic crossover geometry.

3.6. Validity of the harmonic approximation

The harmonic approximation is highly questionable for large molecules. It fails whenever large-amplitude bending and torsional motions are involved in the geometry change, features common in large floppy molecules with rotatable sidechains. Specifically, X-H stretching motions are always anharmonic, but this is not particularly relevant to the spectroscopy of chlorophylls. The generic failure of the harmonic approximation would seem to invalidate fits of observed spectra to products of integrals based on the Huang–Rhys approximation, yet good results are usually obtained throughout molecular spectroscopy. The solution

to this riddle is that the potential energy surface does not need to be harmonic in the *rectilinear* coordinates defined by Eqs (7)–(9), but can be harmonic in more generalized variables provided that the kinetic energy remains nearly harmonic in the new coordinate system [95]. Such coordinates are called *curvilinear* coordinates and assume that the potential energy is harmonic as a function of bending and torsional *bond angles* [96]. Indeed, contributions to spectroscopy arising from the anharmonicity that becomes generated in terms of the kinetic energy (kinetic energy is no longer simply $mv^2/2$) are usually quite small, making their neglect a very useful approximation [95,97]. Use of curvilinear coordinates is not always essential for the modelling of the spectra of chlorophyll-like molecules as it is possible that no significant bond angle or torsional changes occur, though it is required most of the time. Codes which robustly predict the absorption and emission spectra of chlorophyll-like molecules using curvilinear coordinates are available [85].

3.7. Regions of validity of the Condon and Herzberg–Teller approximations

In the spectroscopic treatise of Sponer and Teller [76], three primary sources of spectroscopic intensity are identified: those describable by the Condon approximation (the transition moment is coordinate invariant) [98], the Herzberg–Teller approximation (Eq. (10), the transition moment varies linearly with displacement) [99], and non-adiabatic effects. All three types of contributions are relevant to the spectroscopy of chlorophylls. Nevertheless, using modern diabatic interpretations as will be described shortly, the Herzberg–Teller effect appears as a *consequence* of non–adiabatic coupling rather than as an *independent* quantity. Keeping to simple equations (rather than the general ones [100]), if we only consider the "antisymmetric" modes, harmonic potentials, and ignore Duschinsky rotation, then Eq. (16) can be simplified to:

$$\mathbf{H}_a^{\mathbf{Diabatic}} = \begin{bmatrix} \sum_{ka} \frac{h\nu_{ka}}{2} \Delta Q_{ka}^2 + T\left(\frac{\partial^2}{\partial \mathbf{Q}^2}\right) & 0 & 0 \\ 0 & \Delta E_0 + \sum_{ka} \frac{h\nu_{ka}}{2} \Delta Q_{ka}^2 + T\left(\frac{\partial^2}{\partial \mathbf{Q}^2}\right) & \sum_{ka} \alpha_{ka} Q_{ka} \\ 0 & \sum_{ka} \alpha_{ka} Q_{ka} & \Delta E_0 + \Delta E + \sum_{ka} \frac{h\nu_{ka}}{2} \Delta Q_{ka}^2 + T\left(\frac{\partial^2}{\partial \mathbf{Q}^2}\right) \end{bmatrix}. \quad (18)$$

This can be solved applying perturbation theory to express the transition moment for absorption and emission involving Q_y as

$$\bar{\mu}_{S0,Qy}(\mathbf{Q}) = \bar{\mu}_{S0,Qy}^0 + \sum_{ka} \frac{\alpha_{ka}}{\Delta E} Q_{ka} \bar{\mu}_{S0,Qx}^0. \quad (19)$$

Hence, the nominally *y*-polarized Q_y absorption and emission spectra attain partial *x*-polarized character owing to the non-adiabatic coupling. This represents the Herzberg–Teller parameters in Eq. (10) [101]:

$$\mu_{if,k} = \frac{\alpha_{ka}}{\Delta E} \bar{M}_{S0,Qx}^0. \quad (20)$$

This procedure provides a very useful means for the determination of non-adiabatic couplings from the results of electronic-structure calculations (diabatization), since all that is required is that the transition-moment matrix elements [102,103] are available rather than explicit evaluation of *FD*.

As shown in Fig. 2, the Q_y and Q_x transition moments are not actually perpendicular, and there is no rigorous separation of symmetric and antisymmetric vibrations. Hence, in reality, Eq. (19) embodies interference of Franck–Condon and Herzberg–Teller intensities. This interference manifests differently in absorption and emission and thereby asymmetry is introduced that can mimic the effects of Duschinsky rotation [100,104].

A big picture, therefore, emerges in which the Condon approximation is expected to hold in the absence of Herzberg–Teller effects, and that the Herzberg–Teller approximation is then expected to hold only if the full non-adiabatic effects can be expanded in a perturbation series. We will show that it is possible to interpret the spectra of Pheo-a and BChl-a using the Condon approximation with small contributions from

Herzberg–Teller intensity, whereas for Chl-a, $\frac{\alpha_{ka}}{\Delta E} = \frac{1}{2}$ and zero-point motion in the antisymmetric modes causes Eq. (19) to fail, demanding full treatment of non-adiabatic couplings implementing variational approaches [50,89,105–107]. These non-adiabatic couplings form a hierarchical series, as illustrated in Fig. 3 by dotted lines.

3.8. Diabatic models for spectra embodying non-adiabatic coupling

Diabatic models were first introduced by London in 1932 [108] and provide a way forward in which spectroscopy and kinetics can be conceptualized. These are similar to crude adiabatic models, but instead of applying the crude adiabatic simplifications globally, they are only applied to selected critical aspects and the BO description is applied otherwise. Experimentally, this means categorizing easy-to-interpret features using their BO descriptions, then selecting key aspects of interest for more intense scrutiny. Computationally, diabatic models are usually obtained by taking results from electronic-structure calculations performed by means of the BO approximation, then transforming them into a suitable diabatic representation. The conceptual issue regarding this is that no diabatic transformation is unique and hence arbitrary decisions are usually made. Finding useful a priori schemes for this is a current research challenge, a process known as *diabatization*. The ad hoc introduction of the state energy gap in $\mathbf{H}^{\text{CA2,BOguess}}$ can be interpreted as arising from such a diabatization process where one sees on display both its lack of unique justification and its applicability to the description of a wide range of spectroscopy. Human-inspired diabatization of the 3-state Hamiltonian pertinent to the low-energy Q-band spectroscopy leads to a more general form of Eq. (18):

$$
\mathbf{H}^{\text{Diabatic}} = \begin{bmatrix} V_{S0}(\mathbf{Q}) + T\left(\frac{\partial^2}{\partial \mathbf{Q}^2}\right) & 0 & 0 \\ 0 & V_{Qy}(\mathbf{Q}) + T\left(\frac{\partial^2}{\partial \mathbf{Q}^2}\right) & \sum_{ka} \alpha_{ka} Q_{S0,ka} \\ 0 & \sum_{ka} \alpha_{ka} Q_{S0,ka} & V_{Qx}(\mathbf{Q}) + T\left(\frac{\partial^2}{\partial \mathbf{Q}^2}\right) \end{bmatrix}, \tag{21}
$$

where

$$
V_{S0}(\mathbf{Q}) = \sum_{ks} \frac{h\nu_{S0,ks}}{2}\left(Q_{S0,ks} - Q_{S0,ks,0}\right)^2 + \sum_{ka} \frac{h\nu_{S0,ka}}{2}\Delta Q_{S0,ka}^2,
$$

$$
V_{Qy}(\mathbf{Q}) = \sum_{ks} \frac{h\nu_{S0,ks}}{2}\left(Q_{Qy,ks} - Q_{Qy,ks,0}\right)^2 + \sum_{ka} \frac{h\nu_{Qy,ka}}{2}\Delta Q_{S0,ka}^2, \tag{22}
$$

$$
V_{Qx}(\mathbf{Q}) = \sum_{ks} \frac{h\nu_{S0,ks}}{2}\left(Q_{Qx,ks} - Q_{Qx,ks,0}\right)^2 + \sum_{ka} \frac{h\nu_{Qx,ka}}{2}\Delta Q_{S0,ka}^2.
$$

In these equations, the vibrational modes are partitioned into "symmetric" modes s and "antisymmetric" modes a. Such partitioning can rigorously be applied only to high-symmetry molecule such as benzene and porphyrin. The symmetric and antisymmetric modes are perceived as having very different physical significance in the Hamiltonian (22), as indeed is the case for high-symmetry molecules: only symmetric vibrations generate Huang–Rhys factors, while the antisymmetric modes involve electron-vibration couplings that link Q_x to Q_y. In molecular spectroscopy, such couplings are termed *vibronic* couplings [60,106,107,109–112], but as will be further discussed below, the meaning here has no connection to the meaning of electron-vibration or electron-phonon coupling that arises in the crude adiabatic description of spectroscopy commonly used in solid-state physics [22,26,65,80–83].

Although the partitioning into s and a modes in case of low-symmetry chlorophyllides is only an approximation, $\mathbf{H}^{\text{Diabatic}}$ does provide the language needed to describe the qualitative features observed for their Q-band spectra as it categorizes vibrations into two needed iconic types. One type generates Franck–Condon factors and hence Huang–Rhys vibrational progressions as usually found in electronic spectroscopy; the other type generates the non-adiabatic couplings that mix Q_x with Q_y. Non-adiabatic coupling attributes properties such as spectral polarization to one state that were previously only considered to be appropriate

for the other. Strong non-adiabatic coupling means that the excited states do not behave as if nuclear motion is occurring on a single classical-like potential energy surface. The excited states are then intrinsically quantum in nature, and many features characteristic of molecular spectroscopy no longer apply. A dramatic consequence observed in relation to this is, for example, that the *x*-polarized absorption attributed nominally to Q_x has a *minimum* at the centre of the absorption band [63], not a *maximum* as is demanded by classical spectroscopy controlled by Huang–Rhys factors [58].

Computationally, to obtain spectra from this Hamiltonian, a variety of additional approximations could be introduced, such as neglect of the Duschinsky matrix, treating vibration frequencies as being the same in different electronic states, etc. Such approximations add to the one already introduced that artificially characterizes vibrations as *s* and *a*. In very extensive simulations, this characterization is not essential, and indeed complete diabatic Hamiltonians could be written that allow all vibrations to have some "*a*" character and some "*s*" character. No example of this approach is given here due to the complexity of such representations. They are useful in computational analyses but are too complex for the provision of a basic physical picture for the interpretation of chlorophyll spectroscopic data.

As mentioned above, a weakness of any diabatic description is the arbitrariness of the representation used to construct the Hamiltonian. For example, a 45-degree rotation of the Q_y and Q_x states would depict the *s* modes in terms of linear electron-vibration coupling and the effect of the *a* modes in terms of Franck–Condon type overlaps, seemingly reversing the appropriate notation. In both cases, only the *a*-type modes generate the non-adiabatic coupling matrix elements in the BO representation as rotation of the diabatic basis does not change the BO description or any observable property. However, it is not appropriate to view the diabatic description as fundamentally inferior to the BO description because of this property, as the BO description itself introduces a privileged role for nuclear position over nuclear momentum, something which is not a feature of quantum mechanics. Indeed, arbitrary rotation of position and momentum would destroy the physical meaning of all quantities involved in the BO approximation and yet it would not change the deduced value of any physical observable either, following accurate numerical solution of the resulting Hamiltonian.

The most significant deficiency of the presented form of $\mathbf{H^{Diabatic}}$, and indeed the form of all other models presented, is that they do not explicitly include the Soret states B_y and B_x. Hence, they ignore non-adiabatic coupling especially between Q_x and the Soret states. As indicated later, qualitative evidence for couplings between these states is detected in the spectra of most chlorophyll-like molecules, but it only influences the high-energy spectral tail and consequently has not been a priority for research.

3.9. Molecular spectroscopy from a crude adiabatic perspective

Tradition in solid-state physics [9,22,65,80–84,113] has seen the basic spectroscopic problem expressed in varying crude adiabatic bases rather than the BO basis [78,79]. Instead of starting with the full quantum description and introducing approximations, this approach starts with the simplest possible description, in which all effects appear as some type of coupling, and then building up by adding these couplings one at a time until a model is reached that can interpret observed spectra. The simplest crude adiabatic description ignores all influences that the electronic and nuclear subsystems could exert on each other. For a simple spectroscopic system involving only two states, the resulting Hamiltonian is

$$\mathbf{H^{CA0}} = \begin{bmatrix} T(\frac{\partial^2}{\partial \mathbf{Q}^2}) & 0 \\ 0 & T(\frac{\partial^2}{\partial \mathbf{Q}^2}) \end{bmatrix}. \tag{23}$$

In this case, all electronic wavefunctions are the same, independent of nuclear position and momentum, and the nuclear wavefunctions are sinusoidal functions corresponding to a particle in free space. To improve on this description, the first equivalent harmonic potentials are added to each state and then linear couplings α_k between the electronic and vibrational motions, called *electron-vibration* couplings (also known in this context as *vibronic* couplings), are added to make

$$\mathbf{H^{CA2}} = \begin{bmatrix} \frac{1}{2}\sum_k h\nu_k Q_k^2 + T(\frac{\partial^2}{\partial \mathbf{Q^2}}) & \sum_k \alpha_k Q_k \\ \sum_k \alpha_k Q_k & \frac{1}{2}\sum_k h\nu_k Q_k^2 + T\left(\frac{\partial^2}{\partial \mathbf{Q^2}}\right) \end{bmatrix}. \tag{24}$$

An alternate crude adiabatic approach is to introduce electronic (excitonic) couplings J in the off-diagonal positions instead of the linear vibrational couplings [9,65,83,113]; more pertaining to the combination of these two possibilities will be described later.

Spectra can be evaluated from either type of the crude adiabatic Hamiltonian by direct means, but a simple approach is to introduce the BO approximation to simplify it, obtaining for Eq. (24), without further approximation,

$$\mathbf{H^{CA1,BO}} = \begin{bmatrix} \frac{1}{2}\sum_k h\nu_k\left(Q_k + Q_{k,0}\right)^2 + T(\frac{\partial^2}{\partial \mathbf{Q^2}}) & 0 \\ 0 & \frac{1}{2}\sum_k h\nu_k\left(Q_k - Q_{k,0}\right)^2 + T(\frac{\partial^2}{\partial \mathbf{Q^2}}) \end{bmatrix}, \tag{25}$$

where $Q_{k,0} = \alpha_k/h\nu_k$. This can then immediately be used to generate Huang–Rhys factors, etc., and simulate spectra. As mentioned above, this application of BO approximation is exact and thus its application yields the exact quantum spectrum for the crude adiabatic model that is used to define both the Hamiltonian and its nomenclature.

To provide a realistic description of most molecular spectroscopy, one needs to add another parameter, the energy difference between the two electronic states ΔE_0. In the context of experimental data interpretation, this is usually performed empirically, adding it to the BO-transformed Hamiltonian to make

$$\mathbf{H^{CA2,BOguess}} = \begin{bmatrix} \frac{1}{2}\sum_k h\nu_k\left(Q_k + Q_{k,0}\right)^2 + T(\frac{\partial^2}{\partial \mathbf{Q^2}}) & 0 \\ 0 & \frac{1}{2}\sum_k h\nu_k\left(Q_k - Q_{k,0}\right)^2 + T\left(\frac{\partial^2}{\partial \mathbf{Q^2}}\right) + \Delta E_0 \end{bmatrix}. \tag{26}$$

This Hamiltonian takes the form of a standard one expected within the BO approximation, and thus the whole spectroscopic analysis proceeds smoothly. Nevertheless, there is no justification for adding a parameter that belongs to a crude adiabatic model to the Hamiltonian when re-expressed in BO terms. Hence, for both conceptualizing general molecular spectra and in computational studies, an appealing alternative is to add the energy difference to the original crude adiabatic Hamiltonian, yielding

$$\mathbf{H^{CA3}} = \begin{bmatrix} \frac{1}{2}\sum_k h\nu_k Q_k^2 + T(\frac{\partial^2}{\partial \mathbf{Q^2}}) & \sum_k \alpha_k Q_k \\ \sum_k \alpha_k Q_k & \frac{1}{2}\sum_k h\nu_k Q_k^2 + T\left(\frac{\partial^2}{\partial \mathbf{Q^2}}\right) + \Delta E_0 \end{bmatrix}. \tag{27}$$

Application of the BO approximation to this Hamiltonian *does not* yield $\mathbf{H^{CA2,BOguess}}$, but instead a Hamiltonian depicting a complex ground state that can have either one or two local minima [63,89,114,115]. The trapping of polarons in crystals [83,113,116] is an analogous manifestation of this phenomenon. In this case, the BO transformation is not exact either, meaning that the simple description of spectroscopy that the BO approximation affords no longer fully applies. To proceed, full numerical solution to $\mathbf{H^{CA3}}$ is usually applied, but alternatively the BO approximation could be introduced, directly treating the unwanted couplings that then appear.

Electron-phonon coupling involving intermolecular motions is usually depicted in the same way as are Huang–Rhys factors [58,80–83] in the crude adiabatic description. An important analytical result can be obtained by integrating Eq. (14) assuming a continuous distribution of phonons to reveal

$$\exp\left(-S_{ph}\right) = \frac{I_{ZPL}}{I_{ZPL}+I_{PSB}}, \tag{28}$$

where I_{ZPL} is the intensity of the zero-phonon line, I_{PSB} represents the intensity of its phonon sideband, and S_{ph} is the total number of phonons excited by the transition. This result also holds after inclusion of thermal effects critical to the understanding of phonons. In practice, the shape of the ZPL and its PSB can be sensitive to experimental conditions (e.g, the excitation wavelength in a fluorescence-based measurement) and therefore must be considered on a case-by-case basis [117]. Always some residual inhomogeneous broadening remains, and hence the ZPL shape is usually represented by a Gaussian function. The PSB is then represented by a Lorentzian function, truncated at some (large) band extent to make it integrable.

Understanding even more complex spectroscopic phenomena from the crude adiabatic perspective usually proceeds by adding more terms to $\mathbf{H^{CA3}}$, when and if required. Such terms could include vibrational frequency changes and Duschinsky rotation. Indeed, different vibration frequencies between the two BO states is an inherent property of $\mathbf{H^{CA3}}$, but contributions beyond that, as already perceived, may also be critical. Unfortunately, inclusion of such subtleties in $\mathbf{H^{CA3}}$ quickly becomes unwieldly. The crude adiabatic approach provides an excellent reference frame for the interpretation of spectra in solid-state physics, and has the advantage that the non-adiabatic effects appear quite naturally. On the other hand, it lacks the general simplicity and power of the BO approach and its broader conceptualization of spectroscopy.

3.10. Notation ambiguities

The discussion has raised some ambiguities in nomenclature that have arisen as different communities have focused on different aspects of spectroscopy and hence introduced different models that have formed the basis for spectroscopic nomenclature. The expression "electron-phonon coupling" is not ambiguous as all communities separate out the intermolecular motions from the intramolecular ones, and the same notation arises in each case. Alternatively, the expression "electron-vibration coupling", or equivalently "vibronic coupling", has come to mean "nuclear displacement" to the solid-state physics community [22,26,62,65,80–83] and "non-adiabatic coupling" to the molecular spectroscopic community [60,76,106,109–112,118]. These two aspects of spectroscopy are very different from each other, and both are important for the understanding of spectroscopy and the function of chlorophylls. Indeed, previously we have used "vibronic coupling" to mean nuclear displacement in our work on BChl-a, and to mean non-adiabatic coupling in our work on Chl-a and BPheo-a, focusing on the aspects most relevant at the time. Herein, we do not apply these expressions at all, using instead "Huang–Rhys factors" and "non-adiabatic couplings" to avoid ambiguity. In other modern contexts, the two types of terms are critical to the understanding of coherences observed in fs-ps-timescale quantum interference experiments on photosystems. In this field, resonances associated with Huang–Rhys factors are usually termed "vibrational resonances", whereas those associated with intermolecular non-adiabatic effects are usually termed "vibronic resonances". Related to these issues is the language used for the Herzberg–Teller effect [99], which is usually applied when non-adiabatic couplings are weak and can be treated perturbatively using Eq. (26) [102,103,106,119]. Couplings implicated in chlorophyll spectroscopy are not always weak [63], however, and then the effect is sometimes described as "Herzberg–Teller vibronic coupling" [100,119,120], so as to stress that not all non–adiabatic effects are included in its perturbative approach.

4. ABSORPTION-EMISSION SYMMETRY BREAKING IN THE VIBRATIONAL STRUCTURE OF Q_y

In this section, we consider the Q_y absorption and emission spectra of Pheo-a, BChl-a, and Chl-a, observed in both low resolution and high resolution, examining deviations from mirror symmetry. However, various issues make this a challenge, including the interference of Q_x in the absorption processes, the effects of solvent environment in modifying spectra, and for BChl-a and Chl-a, variations in the ligation of the central magnesium atom that may occur even within the one sample.

We start by considering Pheo-a as for this molecule there is no central magnesium and the Q_x band is sufficiently removed from Q_y for its influence on the properties of interest to be neglected. Some observed low-resolution and high-resolution spectra [121] are shown in Fig. 4, taken at 4.5 K in triethylamine (TEA) glass.

Standard absorption and emission spectra are shown in Fig. 4a. Emission occurs only from the lowest energy state Q_y, displaying an origin band at 669.9 nm, a 0–1 vibrational sideband at 720 nm, and a 0–2 sideband at 747 nm. These features are qualitatively paralleled in absorption at 668.4 nm, 611 nm, and 561 nm. In absorption also, a series of peaks between 541 and 475 nm attributed to Q_x is observed, as well as the absorption attributed to the Soret bands *B* at and beyond 418 nm. Figure 4b shows these spectra after normalization to reveal the intrinsic band shapes, plotted against the frequency difference from the Q_y origin, with the emission spectrum reflected so as to overlap the absorption spectrum. The key feature revealed is that the Q_y absorption and emission spectra are asymmetric, with the 0–1 peaks occurring at different vibrational offsets and displaying different intensities. The insert in the figure shows the spectra fitted to Huang–Rhys models, revealing that the absorption peak at +2800 cm^{-1} is not of Huang–Rhys origin; this deviation from expectation is addressed in the following section. Figure 4b compares the standard low-resolution fluorescence excitation spectrum to the high-resolution 0–1 spectral line intensities obtained using selective excitation. It is clear that the high-resolution and low-resolution spectra depict the same basic features. This is quantified in Table 1 where the absorption end emission reorganization energies deduced from the low-resolution and high-resolution spectra [121] are listed. These are 355 cm^{-1} and 317 cm^{-1} in absorption and 402 cm^{-1} and 395 cm^{-1} in emission, respectively, indicating asymmetry between absorption and emission that is independent of the measurement technique.

For BChl-a, the low-resolution absorption and emission spectra in TEA observed at 4.5 K are reported in Fig. 5, upon either slow or fast cooling of the samples from room temperature [67]. As this chromophore contains a magnesium atom, ligation with the solvent is possible, which depends on the cooling rate. On rapid cooling, the ambient 5-fold coordination (5CO) of magnesium is largely retained, while on slow cooling, species showing 6-fold coordination (6CO) are prevailing. For both species, the qualitative spectral features are mostly similar. This is especially true in emission, with both species displaying Q_y 0–0 origins at 781 nm with associated 0–1 sidebands at 834 nm. In absorption, the corresponding origins are at ~774 nm and ~710 nm, with also weak 0–2 overtone sidebands observed near 650 nm. All of these features appear consistent with what is expected for a basic Huang–Rhys spectral model. In absorption, the Q_x state is apparent as well, showing two peaks with relative intensities that are strongly preparation dependent: the peak at 615–616 nm is assigned to 6CO species whilst that at 584 nm is assigned to 5CO.
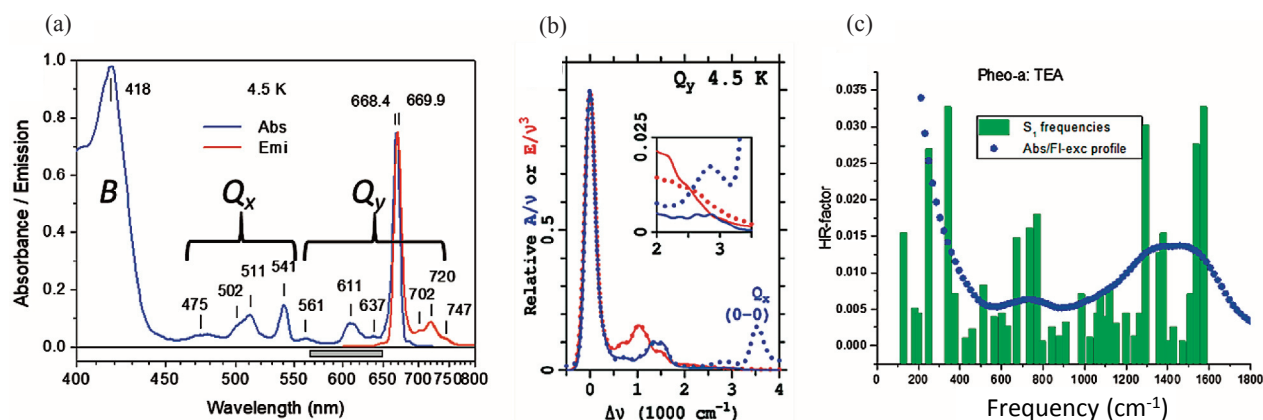

Fig. 4. Aspects of the absorption and emission spectra of Pheo-a in TEA glass at 4.5 K. (a) Unscaled low-resolution spectra, discernible in contributions from the Soret bands *B* as well as from the Q_x and Q_y bands. (b) The Q_y spectra shown as deviations $\Delta v = v - v_{00}$ in absorption (*A*) and $v_{00} - v$ in emission (*E*), normalized to produce the band-shape functions A/v and E/v^3 (dots), and their fit to a Huang−Rhys model (solid lines). (c) Absorption-type spectra as prepared for (b), except that the band-shape function is quantified as an effective Huang−Rhys factor (this is accurate only if bands are non-overlapping) depicting low-resolution and high-resolution fluorescence excitation spectra. Adapted with permission from [122]. Copyright 2019 AIP Publishing.

Table 1. Observed emission and absorption reorganization energies for BChl-a, Chl-a, and Pheo-a in various solvents at different temperatures supporting different magnesium co-ordination numbers, as interpreted from low-resolution and high-resolution spectra

chromophore	solvent	T (K)	CO	low resolution		high resolution	
				λ^A (cm^{-1})	λ^E (cm^{-1})	λ^A (cm^{-1})	λ^E (cm^{-1})
BChl-a	TEA	4.5	6	196[a]	236[a]	~378[ab]	219[ac]
	TEA	4.5	5	335[a]	260[a]		
	TEA	295	5	335[a]	185[a]		
Chl-a	TEA	4.5	5	~300[de]	458[d]		370[d]
	TEA	295	5				413[d]
	wet ether	4.5	5	264[df]	438[d]	262[dg]	
	1-propanol	4.5	6	~420[dh]	~650[dh]		650[d]
	1-propanol	295	5	~490[de]	492[d]		
Pheo-a	TEA	4.5	–	355[i]	402[i]	317[i]	395[i]

a – [67].
b – quantitative analysis available only for 6CO, but the spectra for 5CO are very similar.
c – results for the 5CO species in glycerol water [123] indicate a very similar value.
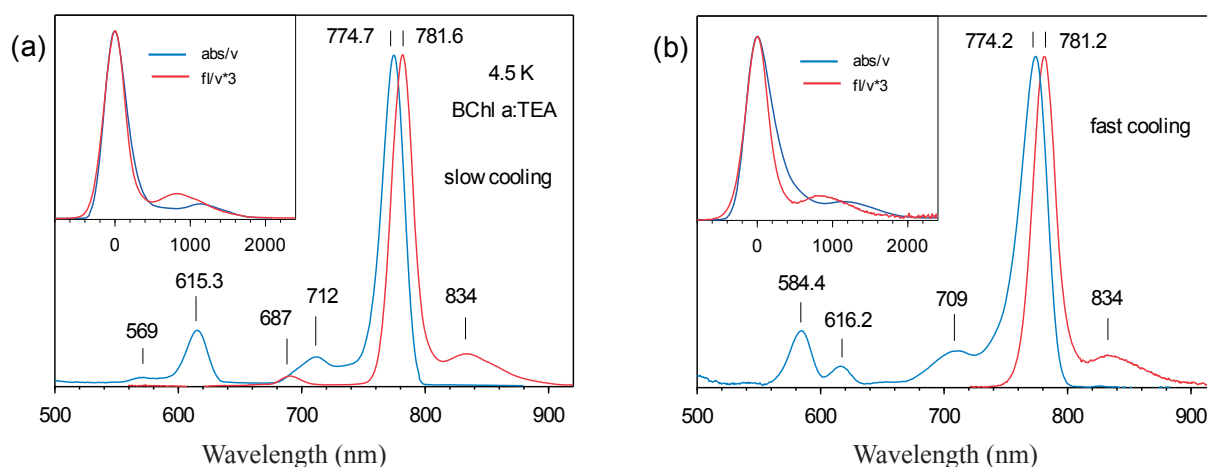d – [124].
e – after approximate removal of the contribution of Q_x using the band shape determined in wet ether [63].
f – the magnesium ligand is water [50], analysis from analytical data inversion of absorption and MCD data [50].
g – data from [42].
h – after approximate removal of contributions from 5CO.
i – [122].

Fig. 5. Absorption (blue line) and fluorescence (red line) spectra at 4.5 K of BChl-a in (a) hexa-coordinated TEA following slow cooling and (b) mostly penta-coordinated TEA following rapid cooling. The fluorescence spectra were excited at around 405 nm. The vertical lines label band positions in nanometers. The insets show the overlap of the absorption and emission spectra in transition dipole moment representation as a function of the frequency differences $\nu - \nu_{00}$ for absorption and $\nu_{00} - \nu$ for emission in wavenumbers. Reprinted with permission from [67]. Copyright 2011 AIP Publishing.

Currently, the feature of primary concern is the asymmetry between the two sets of absorption and emission spectra shown in Fig. 5. This is highlighted in the inserts of the figure, which plots absorption and reflected emission spectra as a function of the change in frequency from the 0–0 transition. Especially for 6CO, the structures of the 0-0-line profiles are very similar up to ca 200 cm^{-1} displacement, indicating that the phonons and/or low-frequency vibrations are such as to produce absorption-emission symmetry. Beyond this, significant deviation occurs, however, with the 0–1 emission maximum appearing near +900 cm^{-1}, whilst the absorption maximum is near +1100 cm^{-1}. The primary question raised is whether these effects arise owing to the vibrational modes changing in frequency between the ground and excited states, or owing to significant redistribution of the intensity of the different modes.

Quantified in terms of the absorption and emission reorganization energies (Table 1), the differences observed in the low-resolution spectra of Fig. 5 mostly indicate significantly enhanced values in emission compared to absorption. In samples of mixed composition, high-resolution techniques often allow contributions from different molecular species to be measured separately, e.g., by selective excitation of only a single species. They also allow the reorganization energies to be separated into contributions from individual vibrational modes, with the Huang−Rhys factors determined for individual 0−1 transitions from the ΔFLN and SHB measurements depicted graphically in Fig. 6. The total reorganization energies implied by this data are listed in Table 1, where they are seen to be in reasonable agreement with the values deduced from low-resolution spectra. The differences between absorption and emission are profound, with the most intense line observed in emission (890 cm^{-1}) being absent in absorption. Hence, it is clear that the differences arise not from small changes in mode frequencies between the ground and excited states, but rather by some processes that redistribute the intensity.

We now turn to the spectra of Chl-a. Similarly to BChl-a, this molecule has a central magnesium that supports a range of ligation environments that influence spectra, see Table 1 [63,124]. However, the interpretation of Chl-a spectra is very difficult due to the strong overlap between the Q_y and Q_x bands. Indeed, two competitive basic assignments persisted over three decades, with each being able to explain some observed spectroscopic features but not all. This was recently resolved with a new assignment that is believed to be capable of explaining all data [63].

Figure 7 shows the key elements involved. Low-resolution emission and absorption spectra are quite asymmetric (Fig. 7a). At the origin +2000 cm^{-1}, only a weak signal is present in the reflected emission spectrum attributable to 0–2 vibrational overtone transitions, whereas relatively strong absorption is detected
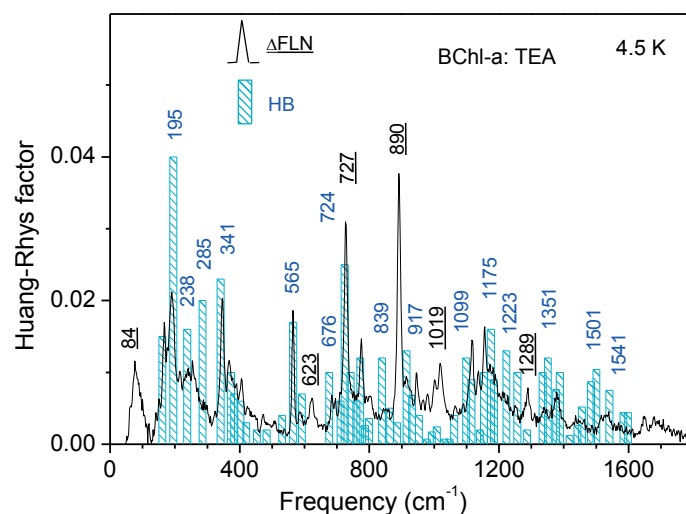

Fig. 6. Comparison of the 6CO BChl-a mode structures related to the Q_y transition, as observed at 4.5 K by ΔFLN (black curve) [67] and SHB (turquoise histogram) [123] methods. The numbers indicate the main vibrational frequencies in wavenumbers. Reprinted with permission from [67]. Copyright 2011 AIP Publishing.
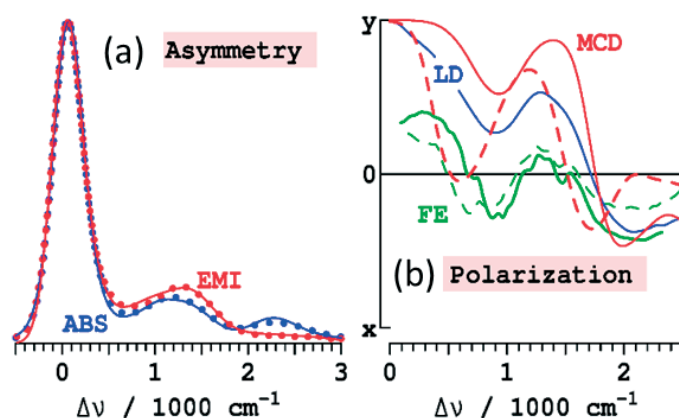
Fig. 7. Observed and interpreted low-resolution spectra for Chl-a in ether at 295 K. (a) Asymmetry between the 5CO absorption $A(\Delta v)v$ and reflected emission $E(-\Delta v)v^3$ spectra from experiment [125] (dots) and from a model including non-adiabatic coupling between Q_x and Q_y [63] (solid lines). (b) Spectral polarizations deduced for 5CO (solid lines) and 6CO (dashed lines) from experimental data [63]: blue – LD [48], red – from analytical data inversion of MCD and absorption spectra [50], green – from polarized fluorescence excitation (FE) [42] interpreted using the $Q_x - Q_y$ non-adiabatic coupling model.

in this region. This effect is directly analogous to the observation of Q_x absorption for Pheo-a and BChl-a without corresponding emission, and hence it is clear that this band is associated with Q_x. A significant difference, however, is that polarization experiments such as linear dichroism (LD) and MCD reveal substantial *x*-polarization to the absorption spanning most of the Q_y spectral range (Fig. 7b), contrary to analogous results for BChl-a and Pheo-a [50,63]. Indeed, a second peak in the *x*-polarized absorption is detected at the origin +800 cm⁻¹, while in classical spectroscopy theory based on the BO approximation, only *one* of the *two x*-polarized peaks can be assigned as Q_x. Based on classical spectroscopy, two possible assignments therefore arise.

The current assignment abandons the BO approximation to view the absorption as arising from quantum interference between the two classical structures, driven by strong non-adiabatic coupling between Q_x and Q_y that cannot be treated using perturbation theories such as the Herzberg–Teller approximation [63]. How this arises is described in detail in Section 6.

In this section we demonstrate that high-resolution spectroscopic techniques are capable of perceiving the key elements of the asymmetry in the Q_y absorption and emission spectra of Chl-a [124], see Fig. 8. Figure 8a shows the ground-breaking high-resolution FE spectrum of Chl-a in wet ether observed by Avarmaa and Rebane [42] in 1985 as well as its modern interpretation [63]. This interprets the spectrum as arising from: (1) the origin band plus fundamental 0–1 vibrational transitions, (2) the 0–2 and higher overtone transitions, (3) the absorption associated with Q_x, and (4) the intrinsic homogeneous linewidth due to phonon interactions. The inset in Fig. 8a demonstrates the deduced phonon-broadened ZPL structure, the blue curve shows the small but yet significant contribution from overtone bands, the purple curve indicates the *x*-polarized contribution, and the red curve refers to the total spectrum after fitting to a set of Huang–Rhys factors describing identified vibrational transitions.

To compare with the absorption-type spectrum shown in Fig. 8a, the observed analogous high-resolution reflected-emission-type spectra are demonstrated in Fig. 8b. These were measured by ΔFLN in two solvents, TEA and 1-propanol. Two qualitative effects are apparent: there is a very large effect of solvent on the vibrational mode intensities (and hence the reorganization energy), and there is very little symmetry between the modes excited in emission and in absorption.
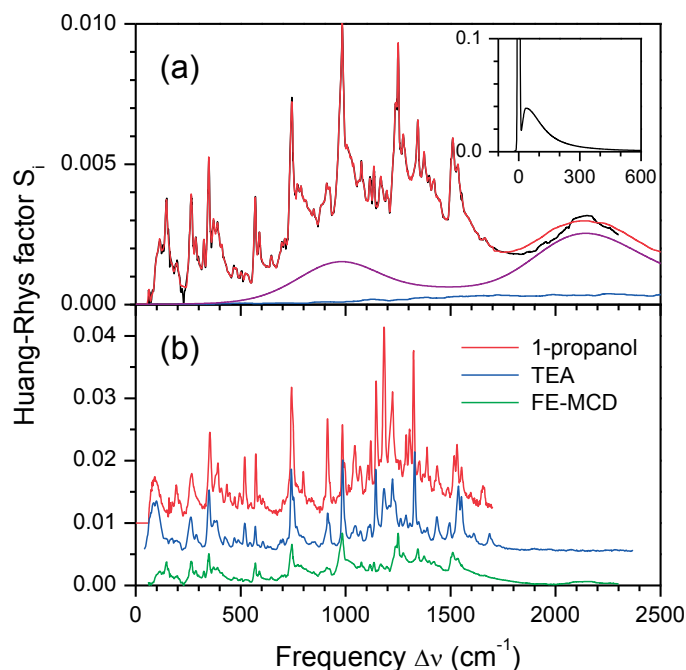
Fig. 8. (a) The normalized high-resolution fluorescence excitation spectrum of Chl-a in wet ether at 4.2 K [42] (black) and its interpretation (red). The fitting curve is evaluated as a sum of a low-resolution x-polarized component (purple, obtained self-consistently along with the MCD spectral fit) and a 236-mode Huang–Rhys component with the assumed ZPL and PSB spectral shape (inset). The blue curve shows the contribution of multiple excitations to the Huang–Rhys spectrum [63]. (b) Comparison of the Chl-a mode structures in 1-propanol (red) and TEA (blue) related to the Q_y transition, as observed at 4.5 K by ΔFLN, with the y-polarized fluorescence excitation profile obtained by subtraction of the purple x-polarized component from the black experimental fluorescence excitation spectrum, as shown in panel (a). For better visibility, the three curves are vertically shifted relative to each other by 0.005 units. For both (a) and (b), the y-scale is such that the value of the Huang–Rhys factor for a vibrational fundamental that is not overlapped by other peaks is given by the peak height.

5. INTERPRETATION OF THE OBSERVED ABSORPTION-EMISSION ASYMMETRY IN TERMS OF THE EFFECTS OF DUSCHINSKY ROTATION

The observed asymmetry in the low-resolution Q_y spectra of BChl-a, Pheo-a, and Chl-a, as quantified by the total absorption and emission reorganization energies, indicates that the same geometrical displacement that occurs between the ground and Q_y states is compatible with quite different potential energy surfaces. If the Duschinsky matrix is ignored (Approx. 3), as well as the BO (Approx. 1), harmonic (Approx. 2), equal-frequency (Approx. 4) and Condon (Approx. 5) approximations are made, then absorption and emission spectra are expected to be symmetric. Therefore, interpreting the experimental asymmetry requires identification of one or more of these assumptions that do not hold.

Differing energy changes in each state could arise owing to anharmonicity, as would be expected if, e.g., electronic excitation led to photodissociation, by significantly reducing the energy of some reactive process. However, this scenario does not likely apply to chlorophyllides as the electronic redistribution associated with excitation (and the related reorganization energy) is small, the property that makes chlorophylls well suited to energy harvesting and transportation processes. Specific calculations provide no evidence either, suggesting that anharmonicities (beyond those describable efficiently using curvilinear coordinates such as peripheral torsional-angle changes) significantly contribute to Q_y spectroscopy, and in particular to the absorption-fluorescence symmetry breaking.

The differing changes in energy in each state could as well arise from changes to the vibration frequencies induced by partial bond breakage. The observed high-resolution spectra give no indication of this as simple

relationships between the high-resolution absorption and emission profiles would then be expected, whereas uncorrelated large-scale rearrangements are depicted by the spectra. Calculations also indicate that frequency changes are minor between the S_0 and Q_y states.

Although evidence can be found in the spectra for the failure of the Condon approximation (such as the observed peak for Pheo-a at a relative energy of +2800 cm^{-1} (Fig. 4b)), and in a much severer form, for the failure of the Born–Oppenheimer approximation (such as the double-peaked Q_x spectrum for Chl-a (Fig. 8a)), none of these effects can explain the observed asymmetry between the high-resolution line intensities revealed in Fig. 8 for Chl-a [124] and in Fig. 6 for BChl-a [67]. The only effect that can have such outcomes is the effect of the Duschinsky rotation matrix that changes the *form* of each vibration as a result of the electronic transition.

How each ground-state mode contributes to excited-state line intensities is specified by Eqs (9), (11), and (12). In particular, Eq. (9) indicates that the displacement ΔQ_l^A that generates the intensity of line l in the excited state arises from frequency-weighted and Duschinsky-weighted (D_{kl}) sums of the analogous displacements ΔQ_k^E that generate the intensities of the emission lines k.

Figure 9 shows the cumulative contribution of each ground-state vibration to this sum, relative to that of the total sum, along with the cumulative contribution of each vibration, D_{kl}^2. Whereas the cumulative contribution to each vibration smoothly increases to one, the contributions to the excited-state displacement manifest quantum interference effects. For the Q_y mode of Chl-a calculated to be at 977 cm^{-1}, only one Duschinsky matrix element is large (Table 2), pertaining to a ground-state mode at an insubstantially different frequency. This mode is strongly displaced and hence it is a significant contributor to vibrational line intensity for both emission-type and absorption-type experiments. Both cumulative functions shown in Fig. 9 acquire the appearance of Heaviside step functions, rising abruptly from near-zero to near-one. The expectation of symmetric absorption and emission spectra assumes that *all* modes of interest have the properties displayed by this mode.

Table 2 considers the modes with the largest reorganization energy observed for S_0 and for Q_y, in turn for Chl-a [124], BChl-a [67], and Pheo-a [122]. For each spectrum, the observed distribution of frequencies and reorganization energies crudely parallels predictions made by CAM-B3LYP calculations, allowing for the mappings listed in the table for observed modes onto calculated modes. The table then lists the largest contributions from the Duschinsky matrix that specify the vibrational modes in Q_y in terms of those in S_0. Inspection of these elements indicates that some modes have a very similar form in the ground and excited states, whereas other modes become strongly mixed.
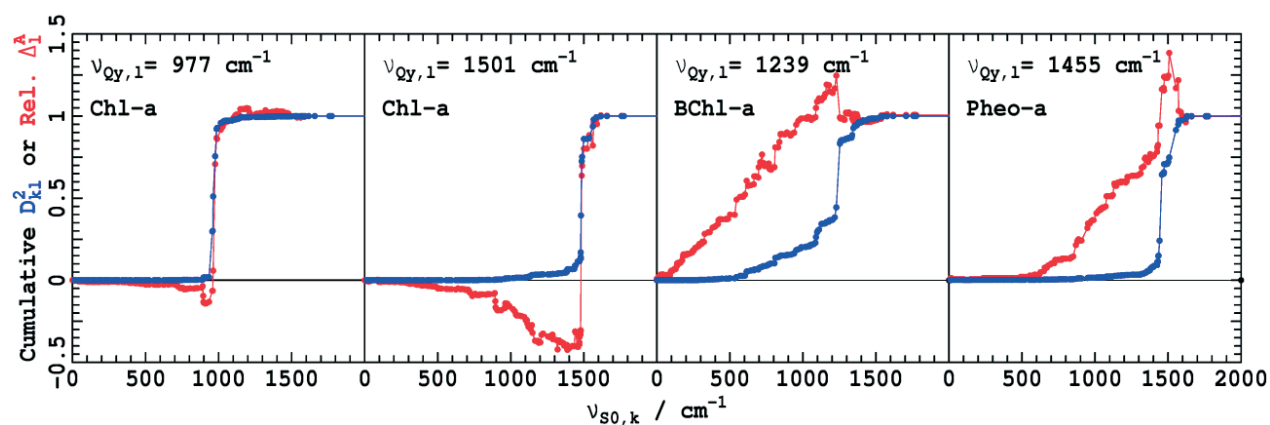

Fig. 9. From Eq. (9), the cumulative weighting from the Duschinsky matrix D_{kl}^2 (blue) and the relative contribution to the displacement ΔQ_l^A that describes the intensity of line l in absorption in terms of contributions from each ground-state mode k (red) [67,122,124].

Table 2. Description of the lines observed at ~ 5 K in absorption (Q_y) or emission (S_0) with the largest reorganization energy λ for Chl-a, BChl-a, and Pheo-a

Q_y obs.		Q_y calc.		Q_y assignment in terms of S_0 modes	S_0 calc.		S_0 obs.	
ν_i	λ_i	ν_i	λ_i		ν_i	λ_i	ν_i	λ_i
Chl-a[a]								
739	11	731,735	20	60% 737, 51% 749, 35% 739	737,739	16	742	12(36)
966	23	977,979	36	87% 977, 45% 986	977	40	986	25(31)
1228	15	1224	47	23% 1211, 60% 1221	1221	35	1223	17(69)
1253	18	1260	15	89% 1262	1262	11	1263	8(10)
1332	18	1329	12	31% 1321, 27% 1348, 15% 1338	1321	37	1329	23(39)
1510	18	1501	15	22% 1481, 33% 1486	1481,1486	24	1519	5(18)
BChl-a[b]								
724	18	719	13	42% 721, 54%727	721,727	11	727	19
845, 858	4	837, 878	8	55% 837, 90% 878	848,877	8	890	25
1154	12	1148	6	82% 1153	1153	8	1158	12
1175	19	1168	10	73% 1183	1183	4	1190	4
1233	16	1239	23	39% 1253, 6% 1229	1253	4	1289	11
1351	16	1348	6	59% 1350, 26% 1346	1350	1		
Pheo-a[c]								
		949	1	21% 948, 76% 952	948	25	985	40
		972	11	80% 974	974	34	1034	36
		992	4	45% 1010, 11% 948	1010	14	1093	31
1294	39	1298	9	27% 1388, 10% 1398	1320	6		
1538	42	1455	31	40% 1458, 17% 1554	1458	2		
1573	51	1554	17	45% 1573, 24% 1587	1573	23	1584	15

a – Chl-a observed for Q_y is from fluorescence excitation in wet ether [42], for S_0 it is from ΔFLN in TEA and in 1-propanol (in parenthesis) [124].
b – BChl-a observed for Q_y is from hole burning in glycerol/water/LDA [123], for S_0 it is from ΔFLN in TEA [67].
c – Pheo-a observed in ether [122].

For Chl-a, BChl-a, and Pheo-a, it has been found to be rare that the excited-state displacement vector is so dominated by a single contribution [67,122,124]. In addition, Fig. 9 shows three other motifs that are commonly predicted by calculations. For the Chl-a Q_y mode calculated to be at 1501 cm^{-1}, again one ground-state vibration dominates the excited-state mode, but in this case very many weakly coupled ground-state modes combine to provide destructive interference that will significantly reduce the excited-state line intensity. For the BChl-a Q_y mode calculated to be at 1239 cm^{-1}, the excited-state line intensity arises from constructive interference between hundreds of ground-state modes, with a more moderate effect of the same kind shown for the BChl-a Q_y mode calculated to be at 1455 cm^{-1}.

The effect of Duschinsky rotation to provide large asymmetry in the spectra of chlorophyllides is made apparent in Table 2, as for the 18 vibrational lines listed that have the largest reorganization energies in either absorption or emission, in 6 cases it is not possible to identify *any* corresponding line in the other spectrum. Indeed, for only one case, the line calculated to be at 977 cm^{-1} in both the ground and excited states of Chl-a, there is a clear correspondence between absorption and emission intensities.

6. NON-ADIABATIC EFFECTS

All of the analysis of chlorophyllides presented so far is based on the two-state harmonic-oscillator uncoupled Born–Oppenheimer description provided by Eq. (26). The absence of coupling allows for ready determination of the potential energy surfaces by quantum chemical means, allowing for straightforward spectral simulations. Nevertheless, many states are implicated in the observed spectroscopy, and Eq. (16) presents a general 3-state model that treats S_0, Q_y, and Q_x on an equal footing. Even this is not sufficiently general to describe all of the observed low-energy spectroscopic processes and, at least, needs to be generalized to an analogous 5-state model containing also B_y and B_x.

We proceed not by evaluating the terms appearing in Eq. (16) by first principles, but instead by introducing the diabatic Hamiltonian $\mathbf{H}_a^{Diabtic}$, Eq. (18), that ignores non-adiabatic couplings with the ground state and assumes that those acting between excited states are proportional to displacements in a few selected modes. The latter are conventionally labelled as *antisymmetric* modes, with Eq. (26) remaining in use for the description of the *symmetric modes*, the modes that generate Huang–Rhys factors and their associated vibrational progressions.

If the ratio of the non-adiabatic coupling to the energy difference between the excited states satisfies the equation $\alpha_{kd}/\Delta E \ll 1$, then the coupling can be treated using perturbation theory, yielding the transition moment profile Eq. (19) for use in simpler 2-state models. In this way, the Herzberg–Teller approximation is generated via the connection with Eq. (20). For most chlorophyllides, with the notable exception of Chl-a, this approximation holds. As a result, it is possible to describe the x-polarized contribution to the Q_y absorption, as revealed most commonly by MCD experiments [50]. This same non-adiabatic coupling transfers y-polarized intensity into the Q_x band. By a similar mechanism, non-adiabatic coupling between Q_x and B_y and/or B_x can significantly alter the absorption band intensity and shape of Q_x. What appears as obvious examples of this effect will include the appearance of the absorption band at 2800 cm^{-1} from the Q_y origin of Pheo-a (Fig. 4b).

The energy gap ΔE between Q_y and Q_x is strongly modulated by chromophore variation and is also solvent dependent, allowing for significant changes to the effect of the non-adiabatic coupling acting between these states [63]. Although traditionally the importance of the non-adiabatic coupling is described in terms of the ratio $\alpha_{kd}/\Delta E$, for absorption spectra the crucial descriptor is in fact $\alpha_{kd}/(\Delta E - h\nu_{ka})$. For Chl-a, the non-adiabatic coupling is only focused on one vibrational mode with $h\nu_{ka} = 1500$ cm^{-1}, with solvent variations modulating ΔE from, e.g. 1640 cm^{-1} in ether to 680 cm^{-1} in isopropanol, and a non–adiabatic coupling of $\alpha_{ka} = 750$ cm^{-1}. Hence, for Chl-a, the Born−Oppenheimer approximation is inappropriate, and any x-polarized spectral simulation based upon it will give very poor results. Thus, the spectra obtained using Huang−Rhys factors and similar methods depict a continuous band with an intense centre that decays to its edges, whereas the non-adiabatic coupling in Chl-a creates an x-polarized band with one absorption maximum in the 1800–2200 cm^{-1} region above the Q_y origin, a second maximum in the region 500–1100 cm^{-1}, and a *minimum* in between [63]. This profile is highlighted in Fig. 8a by purple curve, depicting absorption that is subtracted from the total in order to reveal the Q_y intensity and hence facilitate extraction of high-resolution line intensities and positions, as demonstrated in Fig. 8b.

Using the crude assumption that the non-adiabatic coupling between Q_y and Q_x can be universally described in terms of one antisymmetric mode at 1500 cm^{-1} with a non-adiabatic coupling of 750 cm^{-1}, the x-polarized Q-band intensity can be well described in 32 chlorophyllide/solvent combinations by considering only their effects on the energy gap ΔE [63]. This provides a simple interpretation of a large amount of complex spectroscopic data. The results for 21 examples are listed in Table 3, including the energy gap and the fraction of the total absorption in the Q-band region detected to have x-polarization f_x, and the Q_x to Q_y relaxation time τ. Varying the chemical structure and the solvent shifts this gap within the range 440 $cm^{-1} < \Delta E < 4140$ cm^{-1} for chlorophylls, bacteriochlorophylls, and pheophytins, extending down to –2420 cm^{-1} for the exampled porphyrin derivative. The energy gap for Chl-a in ether, a typical inert solvent, is 1640 cm^{-1}, reducing to 680 cm^{-1} in isopropanol. Of interest, too, is the absorption fraction

Table 3. Fitted values of the unperturbed Q_x-Q_y spacing ΔE (cm^{-1}) and the corresponding fraction f_x of absorption attributed to Q_x for chlorophyllides and related tetrapyrroles, as well as the inferred $Q_x \rightarrow Q_y$ relaxation times $\tau = 1/k$ (fs) [63]

Sample	ΔE	f_x	τ
BChl-a ether	4140	0.21	669[cd]
Chlorin-e6 TME dioxane	3580	0.07	477[d]
Methylpheophorbide-a dioxane	3470	0.12	445[d]
Pheo-a EtOH/MeOH 1.7 K	3380	0.20	419[d]
Pyromethylpheophorbide-a dioxane	3360	0.10	414[d]
BChl-a pyridine	3240	0.22	382[cd]
Ni(II)-Chl-a ether	2750	0.07	231
Zn(II)-Chl-a ether	1990	0.09	122
Chl-a ether	1640	0.10	99[a]
BChl-d ether	1380	0.10	95
ChlZ(D1) PS-II 1.7 K	1350	0.10	95
BChl-c ether	1150	0.16	99
Chl-a pyridine	970	0.17	107[b]
Chl-d MeOH/EtOH 1.7 K	810	0.23	119
Chl-a MeOH/EtOH 1.7 K	820	0.24	122[b]
Chl-a *n*-PrOH 1.8 K	750	0.21	128[b]
Chl-a *i*-PrOH 2.0 K 5CO	1200	0.11	99
Chl-a *i*-PrOH 2.0 K 6CO	680	0.19	134[b]
BChl-d pyridine	710	0.17	128
BChl-c pyridine	440	0.17	161
tetrameso(3,5-di-*t*-butylphenyl) porphyrin	−2420	0.33	−

a – Observed [129] 100±12 fs.
b – Observed [129] times increase with solvent polarity, e.g., 132±10 fs in ethyl acetate, 138±10 fs in THF.
c – Observed 30 fs [130], 100–200 fs [131] or 100–400 fs depending on the environment [132]; 4800 fs in *Prosthecochloris aestuarii* [133].
d – The calculations are likely to overestimate lifetimes at high ΔE [63].

with *x*-polarization. Most models for photosynthetic function include only Q_y, neglecting *x*-polarized absorption. This fraction is detected to range from 0.07 to 0.24 for chlorophyll-type molecules, with the range for Chl-a itself being from 0.10 to 0.24. In the environments in which Q_x is most intensified, its neglect in photosynthesis models may be problematic.

This analysis puts Chl-a into a slightly unique position amongst the chlorophyllides as its absorption cannot be described semi-classically in terms of independent nuclear and electronic motions, as is extremely common throughout spectroscopy of molecules, but instead is highly quantum in nature, manifesting significant quantum entanglement between nuclear and electronic motions [126,127]. The resonance between Q_x and Q_y for Chl-a results in unique ultrafast energy relaxation [63,128]. Table 3 lists the rates predicted using a simple non-adiabatic coupling model [63] parameterized by the deduced energy gaps ΔE, yielding qualitative agreement with observations. There is, however, nothing to suggest that this unique aspect of the spectroscopy of Chl-a is functionally important for photosynthesis.

7. ABSORPTION-EMISSION ASYMMETRY INDUCED BY SOLVENT EFFECTS

The solvation environment affects spectroscopic properties in many ways, including: (1) the phonon interactions (whose properties are critical to the extraction of vibrational properties from high-resolution experiments, such as those listed in Table 2); (2) perturbations to the nuclear and electronic structures arising from intermolecular interactions, both directly with the chlorophyll π-electron system and via interactions such as hydrogen bonding with peripheral functionalities; and (3) by direct interactions with the chromophore through magnesium coordination. For Chl-a and BChl-a, the central magnesium may be either 5CO or 6CO, with Fig. 5 showing low-resolution spectral differences observed for BChl-a in TEA associated with this variation.

Solvent effects observed for Pheo-a [122] are much smaller than those for Chl-a and BCh-a [67,122,124], suggesting that magnesium coordination is a major effect. Therefore, when considering emission-absorption asymmetry, it is critical to compare species with the same magnesium coordination, if not the same solvent and conditions. High-resolution spectroscopic techniques provide a straightforward means for performing this, as selective excitation of each species can be used, even if the sample contains a mixture of differently coordinated molecules.

The comparison of high-resolution emission and absorption lines presented in Table 2 considers species with the same magnesium coordination, with the most intense emission lines for Chl-a additionally presented in both TEA (5CO) and 1-propanol (6CO). The mean average difference in mode frequency for the listed modes in the two solvents is merely 2 cm^{-1}, whereas the line intensities vary by up to a factor of four. The small frequency change is consistent with the basic perceptions that the magnesium coordination has only a relatively minor influence on the primary spectroscopic processes, but such large variations in intensity are unexpected. They can be understood using the hypothesis that absorption-emission symmetry is controlled by aspects of the Duschinsky rotation matrix. As many vibrational modes are involved for molecules the size of chlorophylls, and as subtle effects can readily mix these modes to modulate quantum interference, a relatively minor solvent effect can have profound consequences for line intensities.

8. TOWARDS IMPROVED CALCULATIONS

The calculations used in assigning the basic properties of the spectrum of chlorophyllides [63], and in particular for interpreting the high-resolution absorption and emission spectra of Chl-a [124], BChl-a [67], and Pheo-a [122] involve application of the CAM-B3LYP density functional with the 6-31G* basis set to molecules in the gas phase without magnesium ligation. The key advantages of this approach are that (1) its calculated ground-state vibration frequencies reproduce the highly characterized values for the model compound free-base porphyrin to a root-mean-square error of only 22 cm^{-1}, making it highly appropriate for high-resolution vibrational analyses [67]; (2) its calculated total reorganization energies for both emission and absorption are within a factor of two of experiment and hence it provides a qualitatively useful description of this critical spectroscopic property. Whilst this error is significant, it parallels the variations achievable by solvent variation; (3) the distributions of the reorganization energy into individual vibrational modes that it predicts is sufficient to identify and assign almost all of the significant experimentally observed lines. Finally, CAM-B3LYP predicts a strong ZPL line and weak vibrational sideband, in agreement with experiment. This is not a robust prediction of all computational methods in modern use [67,122,124], and therefore should be thought of as being a significant achievement. Indeed, the results predicted by most computational methods are unreasonable and of no use for the interpretation of experimental data [67,122,124]; the only other method found that could be generally useful is ωB97XD [134], but its errors in calculated reorganization energies have been detected to be 50% larger than those from CAM-B3LYP, while they also share the Kekulé-mode error with CAM-B3LYP (see below).

These are important achievements, making CAM-B3LYP a useful tool for both spectroscopic assignment and the elucidation of the major qualitative features involved. Nevertheless, there is a lack of quantitative precision, with the calculated reorganization energies for the most intense lines sometimes differing from

those observed by a factor of three. The worst-case example found so far for the prediction of vibrational line intensities using CAM-B3LYP pertains to the absorption spectrum of Pheo-a [122]. The observed spectrum and calculated spectrum, both broadened slightly to remove accidental resonance effects, are shown in Fig. 10. The most striking difference between the spectra is the prediction of an intense vibrational line in absorption at 1818 cm^{-1}, a frequency actually greater than any non-hydrogen mode of the molecule [122]. This mode is of Kekulé-type and depicts aromaticity in the excited states. CAM-B3LYP predicts strong non-adiabatic coupling involving this mode that connects the low-lying (n, π*) excited states. These excited states only exist in pheophytins and thus there is no analogous error to be manifested in chlorophylls. As a result of the error, CAM-B3LYP significantly overestimates the reorganization energy and hence the gross spectroscopic properties of Pheo-a. The effect occurs for all computational methods that include some component of the Hartree–Fock exchange operator, and in worst cases, can manifest to be orders of magnitude larger than what is presented here for CAM-B3LYP [122]. If this mode is neglected for Pheo-a, then the CAM-B3LYP calculated line intensities differ from those observed in much the same way as they do for Chl-a [124] and for BChl-a [67]. Errors in individual line intensities can exceed three-fold, but there are similarities in the overall pattern.

An important shortcoming of the strategy depicted in Fig. 10, and being widely applied, is that gas-phase calculations are compared to the observed data obtained in solvents. Significant solvent effects have been observed (depicted in Fig. 8b) that demand detailed explanation, while available approaches are not capable of addressing these issues – for example, calculations with CAM-B3LYP that embody either explicit or implicit solvation produce effects that are small and not qualitatively consistent with observations [67,124]. Considerably improved methods are therefore required.

These results provide the context for understanding computational approaches to the simulation of chlorophyll vibrational spectra at high resolution. Although accurate calculations for molecules the size of chlorophylls have been the domain of density-functional theory, using methods such as CAM-B3LYP, ab initio approaches at various levels of theory have also been applied over the decades, with similar or improved success for the calculation of transition energies that have influenced spectral assignment [75]. Yet, so far, such methods have not been applied to the calculation of Duschinsky rotation effects or to the interpretation of the high-resolution spectroscopy data. This situation is likely to change soon, with advanced applications to chlorophylls currently emerging [135–141].
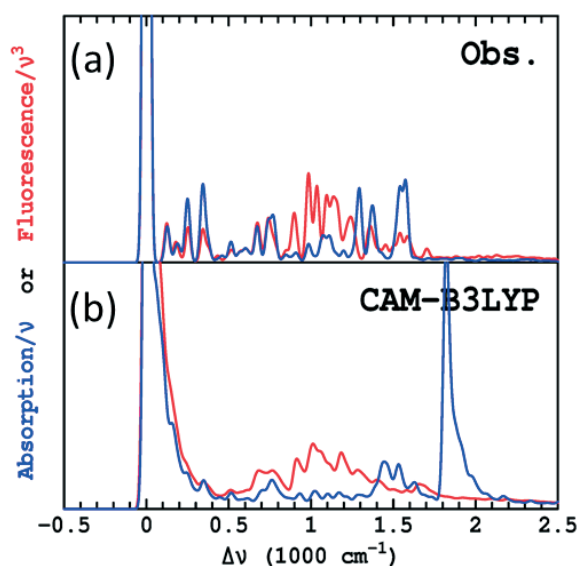

Fig. 10. Observed (in TEA at 4.5 K) and calculated (CAM-B3LYP, gas phase) high-resolution spectra, depicting absorption (blue) and reflected emission (red) for Pheo-a [122]. Both observed and calculated spectra are slightly broadened to avoid accidental resonance effects.

9. MODIFICATIONS OF THE VIBRATIONAL STRUCTURE AND ELECTRON-PHONON COUPLINGS UPON ASSEMBLY INTO PHOTOSYNTHETIC COMPLEXES

Spatial structures of several important photosynthetic pigment-protein complexes are currently refined to near-atomic high resolution [15]. The structures generally display a non-bonded embedding of the pigments into the protein matrix combined with firm fixation of their orientations and conformations by the surrounding network of the nearest amino acid residues.

Next, we will pay attention to cyclic bacteriochlorophyll-a – protein complexes LH2 and LH1 from photosynthetic purple bacteria [142]. The BChl-a pigment chromophores embedded in these integral membrane complexes form distinct circular aggregates, collectively acting as light-harvesting antennas for an efficient catch of solar energy over the broad spectral range [143,144]. While the LH1 or core antennas are directly bound to reaction centres, the transport of optical excitations from peripheral LH2 complexes to the centre complex requires mediation of LH1 complexes.

Excitons are responsible for optical spectra of LH2 and LH1 complexes [68,145–149], well recognized by their characteristic asymmetric absorption bands around 850–870 nm (LH2, traditionally termed the B850 band) and around 870–970 nm (LH1, B875 band). As seen above, the Q_y singlet electronic absorption transition of an individual BChl-a molecule dissolved in organic solvents is located at around 770–780 nm. There is broad consensus that the observed red shift of the exciton absorption bands relative to these of individual chromophores is largely due to exciton couplings between the transition dipoles of closely packed chromophores. The rather great variations detected between the exciton energies of LH2 and LH1 complexes belonging to different species can be explained by a diverse number of pigment chromophores in the respective B850 and B875 aggregates, modified protein surroundings and/or pigment conformations, presence of metal ions, and other reasons that separately or collectively are influencing the pigment-protein and pigment-pigment couplings, thus the energy of excitons.

As is well known [20,22,150], the absorption or emission spectrum of any guest molecule embedded in a chemically inert host matrix at low temperatures consists of a narrow pure electronic ZPL accompanied by a broad PSB and by a large number of localized vibrational lines of pigment origin with the same lineshape as the ZPL. The shape of the so-called homogeneously broadened spectrum contains valuable information about dynamical coupling between the guest and host entities. In many cases, the homogeneous fine structure is difficult to recognize because of the disorder broadening, caused by heterogeneities of the local protein matrix surrounding the pigment chromophores. Also, identical pigment molecules in different protein binding pockets may assume diverse conformations. The matrix induced variations of the pigment-protein and pigment-pigment interactions lead to the mixing of different exciton levels and lifting of their energetic degeneracy as well as to the redistribution of oscillator strength to nearby states [12,68,147,151,152].

Figure 11 demonstrates the ordinary low-resolution fluorescence and high-resolution ΔFLN spectra of BChl-a embedded in various selected solid environments such as TEA glass, Fenna– Matthews–Olson (FMO) protein complex from *Chlorobium tepidum*, and LH2 and LH1 protein complexes from *Rhodobacter sphaeroides* [142]. The spectrum of BChl-a in TEA can be considered as a reference, representing an isolated molecule; the BChl-a pigment chromophores loosely contained in the FMO protein represent a weakly coupled exciton system; the BChl-a chromophores in closely coupled circular arrangements of B850 in LH2 and B875 in LH1 form strongly coupled exciton systems.

As shown above, fine-structured spectra were revealed in all cases. However, the spectra for excitonically uncoupled/weakly coupled (BChl-a: TEA or FMO) and strongly coupled (LH2 or LH1) systems appear very different. The vibrational structure profoundly evident in systems of localized excitations almost vanishes in exciton systems. This is in contrast with the coupling to phonons, which rather dramatically enhances in LH2 and LH1 complexes. In theory, both the vibrational and electron-phonon couplings are expected to decrease with increasing exciton coupling [153–155]. The unexpected boost of the electron-phonon coupling was explained in [142] by exciton self-trapping, promoted by mixing of molecular exciton states with the charge transfer states between the adjacent chromophores in the tightly packed B850 and B875 arrangements.
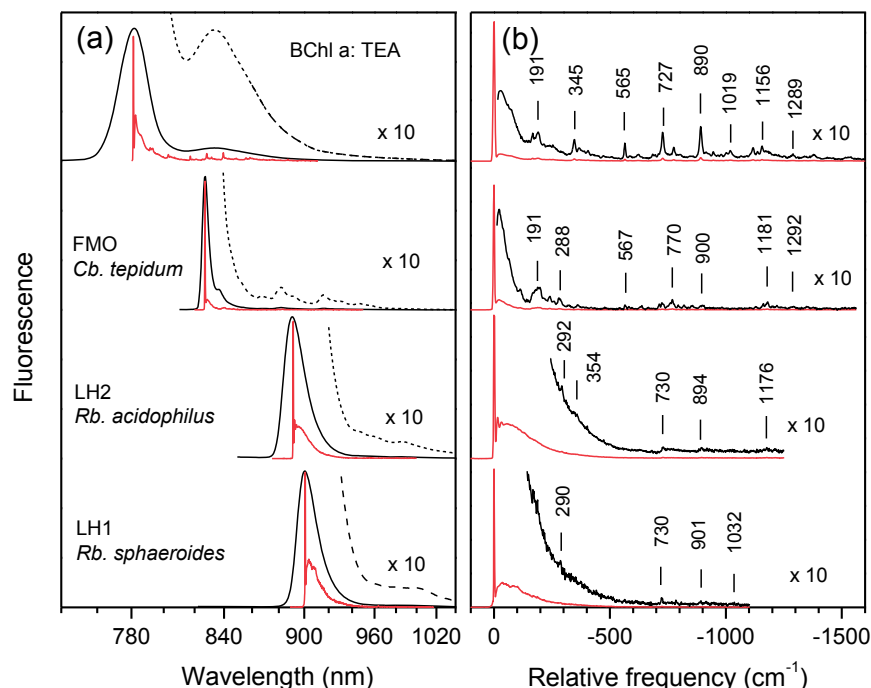
Fig. 11. (a) Comparison of the low-resolution (black line) and high-resolution (red line) fluorescence spectra of BChl-a in frozen solution of TEA and in three different light-harvesting complexes as indicated. The peak-normalized spectra recorded at 4.5 K are presented on the reciprocal wavelength (energy) scale. Shown with dashed lines are the 10-fold amplified tails of the low-resolution spectra. (b) Peak-normalized ΔFLN spectra of the same samples on the relative wavenumber scale; vertical lines label selected vibrational mode frequencies in the ground electronic state. Adapted with permission from [142]. Copyright 2014 AIP Publishing.

10. CONCLUDING REMARKS AND AN OVERVIEW OF ESTONIAN SCIENCE AND COLLABORATION

The spectroscopy of chlorophylls as well as its significance for photosynthetic function are complex multi-disciplinary issues, demanding state-of-the-art high-resolution experimentation, conceptual frameworks, computational predictions, and experimental interpretations. The conceptual foundations of spectroscopy were established in the first 15 years of quantum mechanics and adopted uniformly in the 1940s [76]. Nevertheless, various challenges subsequently resulted in a different conceptual basis and hence notations being developed in Chemical Spectroscopy and in Materials Spectroscopy, with critical concepts such as "vibronic coupling" acquiring very different meanings in the two fields. Unfortunately, both sets of developments are required to understand chlorophyll spectroscopy. The basic underlying difference is that the crude adiabatic approximation is mostly used to describe the spectroscopy of materials, whereas the Born–Oppenheimer approximation is mostly used to describe the spectroscopy of molecules and it also forms the basis for all electronic-structure calculations.

   In this review, we present a re-unified conceptual framework that allows all features associated with chlorophyll spectroscopy to be described by means of unambiguous notations, also providing a basis for the interpretation of much of the previous literature in the field. This basis makes it possible to understand the changes in chlorophyll spectroscopy as it is moved from the gas phase into various solutions and then to in situ in photosynthetic protein matrices at any temperature of the system. The immediate effect of the environment is modulation of the energies of various excited states. Such energy modulations are important functionally as they can be used by nature to optimize chromophores for different applications. Specifically, the environmental modulation of the energy gap between the Q_x and Q_y states significantly affects the

perceived spectra and the rates of reactions such as internal conversion. Environmental effects can also have profound effects on the Q_x absorption intensity, taking it from negligible to significant.

A rather unique spectroscopic feature of Chl-a was detected to be that its *x*-polarized *Q*-band absorption cannot be described at all using the Born–Oppenheimer approximation as it arises from independent classical vibrational motions on individual potential energy surfaces. The Born–Oppenheimer approximation demands that absorption and emission be maximal near the band centre, whereas Q_x absorption in Chl-a has a minimal at the band centre, with maxima located on each side. This interpretation resolved 50 years of ambiguities associated with conflicting traditional Born–Oppenheimer based interpretations of a very wide range of observed spectroscopy data. *Q*-band light absorption by Chl-a is an intrinsically quantum phenomenon. This effect, however, has no recognized consequence for photosynthetic function.

Overall, one of the most significant findings was the discovery and characterization of profound asymmetry between the absorption and emission spectra of chlorophyll-like molecules. This is an unusual and unexpected effect that, even more surprisingly, was found to be extremely environment sensitive. Its simple interpretation in terms of subtle quantum interference effects manifested by Duschinsky rotation of the form of the vibrational motions as a result of electronic excitation provides a wide-ranging understanding. As regards photosynthetic function, this discovery means that any absorption by molecules in vibrational sidebands will re-emit at different energies to that which was originally absorbed, eventually limiting coherence in exciton transport.

This work provides an overview of significant contributions to the understanding of photosynthesis made in Estonia, dating back over a century to the pioneering efforts of Mikhail Tsvet (1872–1919) [156]. At its core, it involves the invention of high-resolution spectroscopic techniques such as SHB [24] in the 1970s, high-resolution fluorescence excitation in the 1980s [26,42], and ΔFLN in the 2000s [30,31], involving four generations of scientists. These techniques, developed under the auspices of the Estonian Academy of Science, are widely applicable throughout condensed-matter spectroscopy. Over the last decade, this research initiative has broadened to involve international collaboration, in particular with research performed under the auspices of the Australian Academy of Science. This embraces an extensive tradition in the development of conceptual understanding [157,158], electronic structure theory including the invention of the ab initio calculation strategy [69] and the first practical methods capable of calculating chlorophyll spectroscopy [159], as well as computational strategies for modelling non-adiabatic coupling [101,105,106,110] and related methods for understanding photosynthetic function [160]. Perhaps the ultimate achievement of this collaboration was the assignment of the spectrum of Chl-a, ending 50 years of debate [63].

ACKNOWLEDGEMENTS
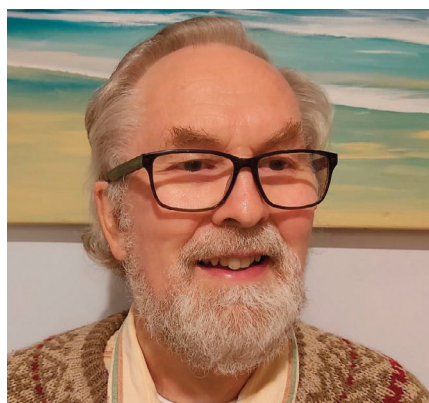
Jeff Reimers completed honours in chemical spectroscopy (1978) and a PhD in molecular physics (1982) at the Australian National University. His scientific contributions include works in the fields of chemical theory, molecular electronics, photosynthesis, and nanophotonics. He is currently employed by Shanghai University and the University of Technology Sydney as part of a collaborative arrangement, being Director of the International Centre for Quantum and Molecular Structures, Shanghai University. He is a Fellow of the Australian Academy of Science, with awards including the H.G. Smith Medal of the Royal Australian Chemical Institute and the Shanghai Magnolia Medal.

Margus Rätsep is an Associate Professor at the Institute of Physics, University of Tartu. He studied physics at the University of Tartu, and obtained his PhD in 1991. He has worked as a Postdoctoral Fellow at Ames Laboratory at Iowa State University (USA) and as a Visiting Scientist at Laboratoire Aimé Cotton, CNRS (France). He is an expert in high-resolution spectral hole-burning and fluorescence line-narrowing spectroscopy. Currently, he works on elucidating the mechanisms of light harvesting and energy transfer on photosynthetic bacteria.

Juha Matti Linnanto (b.1970) received his PhD (physical chemistry) in 2012 from the University of Jyväskylä. His research interests cover various aspects of theory and modelling of electronic, optical, structural and transport properties of photosynthetic pigments, pigment-protein complexes, self-aggregates, dendrimers and metal-organic compounds. Currently he is an Associate Professor at the Laboratory of Biophysics of the Institute of Physics, University of Tartu.

Professor Arvi Freiberg received his PhD in solid state physics from the Estonian Academy of Sciences (1976) and DSc degree from the Latvian Academy of Sciences (1986). His scientific contribution belongs to the fields of ultrafast and spectrally selective spectroscopy of molecular matter, biophysics of photosynthesis, and high-pressure biospectroscopy. As a former Director of the Institute of Physics of the Estonian Academy of Sciences and a Chair Professor of the Department of Biophysics and Plant Physiology of the University of Tartu, he is currently running the Biophysics Laboratory at the Institute of Physics of the University of Tartu, also serving as a Vice-President of the Estonian Academy of Sciences.

REFERENCES

1. Blankenship, R. E. *Molecular Mechanisms of Photosynthesis*. Blackwell Science, Oxford, 2002.
2. Grimm, B., Porra, R. J., Rüdiger, W. and Scheer, H. (eds). *Chlorophylls and Bacteriochlorophylls. Biochemistry, Biophysics, Functions and Applications*. Springer, Dordrecht, 2006.
3. Gurinovich, G., Sevchenko, A. and Solov'ev, K. Spectroscopy of chlorophyll and related compounds. *U. S. Atomic Energy Commission Translation Series*, 1971.
4. May, V. and Kühn, O. *Charge and Energy Transfer Dynamics in Molecular Systems*. Wiley–VCH, Berlin, 2000.
5. van Amerongen, H., Valkunas, L. and van Grondelle, R. *Photosynthetic Excitons*. World Scientific, Singapore, 2000.

6. Duysens, L. N. M. *Transfer of excitation energy in photosynthesis*. PhD thesis. State University of Utrecht, Netherlands, 1952.

7. Seely, G. R. Energy transfer in a model of the photosynthetic unit of green plants. *J. Theor. Biol.*, 1973, **40**(1), 189–199.

8. Bloembergen, N., Purcell, E. M. and Pound, R. V. Relaxation effects in nuclear magnetic resonance absorption. *Phys. Rev.*, 1948, **73**, 679–712.

9. Förster, T. Zwischenmolekulare Energiewanderung und Fluoreszenz. *Ann. Phys.*, 1948, **437**(2), 55–75.

10. Renge, I. and Mauring, K. Spectral shift mechanisms of chlorophylls in liquids and proteins. *Spectrochim. Acta A Mol. Biomol. Spectrosc.*, 2013, **102**, 301–313.

11. Krawczyk, S. The effects of hydrogen bonding and coordination interaction in visible absorption and vibrational spectra of chlorophyll *a*. *Biochim. Biophys. Acta*, 1989, **976**, 140–149.

12. Freiberg, A. and Trinkunas, G. Unraveling the hidden nature of antenna excitations. In *Photosynthesis in Silico: Understanding Complexity from Molecules to Ecosystems* (Laisk, A., Nedbal, L., Govindjee, eds). Springer, Dordrecht, 2009, 55–82.

13. Jang, S. J. and Mennucci, B. Delocalized excitons in natural light-harvesting complexes. *Rev. Mod. Phys.*, 2018, **90**(3), 035003.

14. Song, K. S. and Williams, R. T. *Self-Trapped Excitons*. Springer, Berlin, Heidelberg, New York, 1992.

15. Reimers, J. R., Biczysko, M., Bruce, D., Coker, D. F., Frankcombe, T. J., Hashimoto, H. et al. Challenges facing an understanding of the nature of low-energy excited states in photosynthesis. *Biochim. Biophys. Acta Bioenerg.*, 2016, **1857**(9), 1627–1640.

16. Cupellini, L., Caprasecca, S., Guido, C. A., Müh, F., Renger, T. and Mennucci, B. Coupling to charge transfer states is the key to modulate the optical bands for efficient light harvesting in purple bacteria. *J. Phys. Chem. Lett.*, 2018, **9**(23), 6892–6899.

17. Shafizadeh, N., Ha-Thi, M. H., Soep, B., Gaveau, M. A., Piuzzi, F. and Pothier, C. Spectral characterization in a supersonic beam of neutral chlorophyll *a* evaporated from spinach leaves. *J. Chem. Phys.*, 2011, **135**, 114303.

18. Kjær, C., Gruber, E., Nielsen, S. B. and Andersen, L. H. Color tuning of chlorophyll *a* and *b* pigments revealed from gas-phase spectroscopy. *Phys. Chem. Chem. Phys.*, 2020, **22**, 20331–20336.

19. Sild, O. and Haller, K. (eds). *Zero-Phonon Lines and Spectral Hole Burning in Spectroscopy and Photochemistry*. Springer, Berlin, Heidelberg, 1988.

20. Osad'ko, I. S. *Selective Spectroscopy of Single Molecules*. Springer, Berlin, Heidelberg, 2003.

21. Barkai, E., Jung, Y. J. and Silbey, R. Theory of single-molecule spectroscopy: beyond the ensemble average. *Annu. Rev. Phys. Chem.*, 2004, **55**, 457–507.

22. Rebane, K. K. *Impurity Spectra of Solids*. Plenum Press, New York, 1970.

23. Szabo, A. Laser-induced fluorescence-line narrowing in ruby. *Phys. Rev. Lett.*, 1970, **25**(14), 924–926.

24. Gorokhovskii, A. A., Kaarli, R. K. and Rebane, L. A. Hole burning in the contour of a pure electronic line in a Shpol'skii system. *JETP Lett.*, 1974, **20**(7), 474–479.

25. Kharlamov, B. M., Personov, R. I. and Bykovskaya, L. A. Stable ʿgap' in absorption spectra of solid solutions of organic molecules by laser irradiation. *Opt. Commun.*, 1974, **12**(2), 191–193.

26. Rebane, K. K. and Avarmaa, R. A. Sharp line vibronic spectra of chlorophyll and its derivatives in solid solutions. *Chem. Phys.*, 1982, **68**(1–2), 191–200.

27. Rebane, K. K. Purely electronic zero–phonon line as the foundation for high resolution matrix spectroscopy, single impurity molecule spectroscopy, persistent spectral hole burning. *J. Lumin.*, 2002, **100**(1–4), 219–232.

28. Jaaniso, R. V. and Avarmaa, R. A. Measurement of the inhomogeneous distribution function and homogeneous spectra of an impurity molecule in a glassy matrix. *J. Appl. Spectrosc.*, 1986, **44**(4), 365–370.

29. Fünfschilling, J., Glatz, D. and Zschokke-Gränacher, I. Hole-burning spectroscopy as a tool to eliminate inhomogeneous broadening. *J. Lumin.*, 1986, **36**, 85–92.

30. Rätsep, M. and Freiberg, A. Resonant emission from the B870 exciton state and electron–phonon coupling in the LH2 antenna chromoprotein. *Chem. Phys. Lett.*, 2003, **377**(3–4), 371–376.

31. Rätsep, M. and Freiberg, A. Electron–phonon and vibronic couplings in the FMO bacteriochlorophyll *a* antenna complex studied by difference fluorescence line narrowing. *J. Lumin.*, 2007, **127**(1), 251–259.

32. Pieper, J., Artene, P., Rätsep, M., Pajusalu, M. and Freiberg, A. Evaluation of electron–phonon coupling and spectral densities of pigment–protein complexes by line-narrowed optical spectroscopy. *J. Phys. Chem. B*, 2018, **122**(40), 9289–9301.

33. Osad'ko, I. S. Determination of electron-phonon coupling from structured optical spectra of impurity centers. *Sov. Phys. Usp.*, 1979, **22**(5), 311.

34. Gooijer, C., Ariese, F. and Hofstraat, J. W. (eds). *Shpol'skii Spectroscopy and Other Site-Selective Methods*. John Wiley & Sons, New York, NY, 2000.

35. Orrit, M., Bernard, J. and Personov, R. I. High-resolution spectroscopy of organic molecules in solids: from fluorescence line narrowing and hole burning to single molecule spectroscopy. *J. Phys. Chem.*, 1993, **97**(40), 10256–10268.

36. Jankowiak, R., Reppert, M., Zazubovich, V., Pieper, J. and Reinot, T. Site selective and single complex laser-based spectroscopies: A window on excited state electronic structure, excitation energy transfer, and electron-phonon coupling of selected photosynthetic complexes. *Chem. Rev.*, 2011, **111**(8), 4546–4598.

37. Naumov, A. V., Gorshelev, A. A., Vainer, Y. G., Kador, L. and Köhler, J. Impurity spectroscopy at its ultimate limit: relation between bulk spectrum, inhomogeneous broadening, and local disorder by spectroscopy of (nearly) all individual dopant molecules in solids. *Phys. Chem. Chem. Phys.*, 2011, **13**(5), 1734–1742.

38. Naumov, A. V. Low-temperature spectroscopy of organic molecules in solid matrices: from the Shpol'skii effect to laser luminescent spectromicroscopy for all effectively emitting single molecules. *Phys.-Uspekhi*, 2013, **56**(6), 605–622.

39. Purchase, R. and Völker, S. Spectral hole burning: examples from photosynthesis. *Photosynth. Res.*, 2009, **101**, 245–266.

40. Freiberg, A. and Garab, G. Basic optical spectroscopy for light harvesting. In *Light Harvesting in Photosynthesi*s (Groce, R., van Grondelle, R., van Amerongen, H. and van Stokkum, I., eds). CRC Press, Boca Raton, 2018, 381–426.

41. Renge, I., Mauring, K. and Avarmaa, R. High-resolution optical spectra in vivo: Photoactive protochlorophyllide in etiolated leaves at 5 K. *Biochem. Biophys. Acta*, 1984, **766**, 501–504.

42. Avarmaa, R. A. and Rebane, K. K. High-resolution optical spectra of chlorophyll molecules. *Spectrochim. Acta A Mol. Biomol. Spectrosc.*, 1985, **41**(12), 1365–1380.

43. Renge, I., Mauring, K. and Avarmaa, R. A. Site-selection optical spectra of bacteriochlorophyll and bacteriopheophytin in frozen solutions. *J. Lumin.*, 1987, **37**, 207–214.

44. Avarmaa, R. A. and Rebane, K. K. Zero-phonon lines in spectra of chlorophyll-type molecules in low-temperature solid matrices. *Sov. Phys. Usp.*, 1988, **154**(3), 433–458.

45. Gouterman, M. and Stryer, L. Fluorescence polarization of some porphyrins. *J. Chem. Phys.*, 1962, **37**, 2260–2266.

46. Houssier, C. and Sauer, K. Circular dichroism and magnetic circular dichroism of the chlorophyll and protochlorophyll pigments. *J. Am. Chem. Soc.*, 1970, **92**(4), 779–791.

47. Deroche, M. E. and Briantais, J. M. Absorption spectra of chlorophyll forms, β-carotene and lutein in freeze–dried chloroplasts. *Photochem. Photobiol.*, 1974, **19**(3), 233–240.

48. Fragata, M. U., Nordén, B. and Kurucsev, T. Linear dichroism (250–700 nm) of chlorophyll *a* and pheophytin *a* oriented in a lamellar phase of glycerylmonooctanoate/H_2O. Characterization of electronic transitions. *Photochem. Photobiol.*, 1988, **47**(1), 133–143.

49. Umetsu, M., Wang, Z.-Y., Kobayashi, M. and Nozawa, T. Interaction of photosynthetic pigments with various organic solvents: Magnetic circular dichroism approach and application to chlorosomes. *Biochem. Biophys. Acta Bioenerg.*, 1999, **1410**(1), 19–31.

50. Reimers, J. R., Cai, Z.–L., Kobayashi, R., Rätsep, M., Freiberg, A. and Krausz, E. The role of high-level calculations in the assignment of the Q-band spectra of chlorophyll. *AIP Conf. Proc.*, 2014, **1618**(18), 18–22.

51. Bauman, D. and Wrobel, D. Dichroism and polarized fluorescence of chlorophyll *a*, chlorophyll *c* and bacteriochlorophyll *a* dissolved in liquid crystals. *Biophys. Chem.*, 1980, **12**(1), 83–91.

52. Song, Y., Schubert, A., Maret, E., Burdick, R. K., Dunietz, B. D., Geva, E. and Ogilvie, J. P. Vibronic structure of photosynthetic pigments probed by polarized two-dimensional electronic spectroscopy and *ab initio* calculations. *Chem. Sci.*, 2019, **10**(35), 8143–8153.

53. Sundholm, D. Density functional theory calculations of the visible spectrum of chlorophyll *a*. *Chem. Phys. Lett.*, 1999, **302**(5–6), 480–484.

54. Jusélius, J. and Sundholm, D. The aromatic pathways of porphins, chlorins and bacteriochlorins. *Phys. Chem. Chem. Phys.*, 2000, **2**(10), 2145–2151.

55. Pajusalu, M., Kunz, R., Rätsep, M., Timpmann, K., Köhler, J. and Freiberg, A. Unified analysis of ensemble and single–complex optical spectral data from light-harvesting complex-2 chromoproteins for gaining deeper insight into bacterial photosynthesis. *Phys. Rev. E*, 2015, **92**(5), 052709.

56. Gouterman, M. Spectra of porphyrins. *J. Mol. Spectrosc.*, 1961, **6**, 138–163.

57. Gouterman, M., Wagnière, G. H. and Snyder, L. C. Spectra of porphyrins: Part II. Four orbital model. *J. Mol. Spectrosc.*, 1963, **11**, 108–127.

58. Huang, K. and Rhys, A. Theory of light absorption and non-radiative transitions in *F*-centres. *Proc. Math. Phys. Eng. Sci.*, 1950, **204**(1078), 406–423.

59. de Jong, M., Seijo, L., Meijerink, A. and Rabouw, F. T. Resolving the ambiguity in the relation between Stokes shift and Huang–Rhys parameter. *Phys. Chem. Chem. Phys.*, 2015, **17**(26), 16959–16969.

60. Fulton, R. L. and Gouterman, M. Vibronic coupling. I. Mathematical treatment for two electronic states. *J. Chem. Phys.*, 1961, **35**, 1059–1071.

61. Piepho, S. B. and Schatz, P. *Group Theory in Spectroscopy with Applications to Magnetic Circular Dichroism*. Wiley, New York, NY, 1983.

62. Fischer, G. *Vibronic Coupling: the Interaction between the Electronic and Nuclear Motions.* Academic Press, London, Orlando, 1984.

63. Reimers, J. R., Cai, Z.–L., Kobayashi, K., Rätsep, M., Freiberg, A. and Krausz, E. Assignment of the *Q*-bands of the chlorophylls: coherence loss via Q_x-Q_y mixing. *Sci. Rep.*, 2013, **3**, 2761.

64. Duschinsky, F. On the interpretation of electronic spectra of polyatomic molecules. *Acta Physicochim. USSR*, 1937, **7**, 551.

65. Davydov, A. S. *Theory of Molecular Excitons*. Plenum Press, New York, NY, 1971.

66. Linnanto, J. and Korppi–Tommola, J. Quantum chemical simulation of excited states of chlorophylls, bacteriochlorophylls and their complexes. *Phys. Chem. Chem. Phys.*, 2006, **8**(6), 663–687.

67. Rätsep, M., Cai, Z.-L., Reimers, J. R. and Freiberg, A. Demonstration and interpretation of significant asymmetry in the low-resolution and high-resolution Q_y fluorescence and absorption spectra of bacteriochlorophyll *a*. *J. Chem. Phys.*, 2011, **134**(2), 024506.

68. Cogdell, R. J., Gall, A. and Köhler, J. The architecture and function of the light-harvesting apparatus of purple bacteria: from single molecules to in vivo membranes. *Q. Rev. Biophys.*, 2006, **39**(3), 227324.

69. Parr, R. G., Craig, D. P. and Ross, I. G. Molecular orbital calculations of the lower excited electronic levels of benzene, configuration interaction included. *J. Chem. Phys.*, 1950, **18**(12), 1561–1563.

70. Norden, B., Fragata, M. and Kurucsev, T. X- and Y-polarized spectra of chlorophyll *a* and pheophytin *a* in the red region: resolution enhancement and Gaussian deconvolution. *Aust. J. Chem.*, 1992, **45**(10), 1559–1570.

71. van Zandvoort, M. A. M. J., Wróbel, D., Lettinga, P., van Ginkel, G. and Levine, Y. K. The orientation of the transition dipole moments of chlorophyll *a* and pheophytin *a* in their molecular frame. *Photochem. Photobiol.*, 1995, **62**(2), 299–308.

72. Kleima, F. J., Hofmann, E., Gobets, B., van Stokkum, I. H. M., van Grondelle, R., Diederichs, K. and van Amerongen, H. Förster excitation energy transfer in peridinin-chlorophyll-*a*-protein. *Biophys. J.*, 2000, **78**(1), 344353.

73. Simonetto, R., Crimi, M., Sandonà, D., Croce, R., Cinque, G., Breton, J. and Bassi, R. Orientation of chlorophyll transition moments in the higher-plant light-harvesting complex CP29. *Biochem.*, 1999, **38**(40), 12974–12983.

74. Cai, Z.-L., Sendt, K. and Reimers, J. R. Failure of density-functional theory and time-dependent density-functional theory for large extended π systems. *J. Chem. Phys.*, 2002, **117**(12), 5543–5549.

75. Cai, Z.-L., Crossley, M. J., Reimers, J. R., Kobayashi, R. and Amos, R. D. Density functional theory for charge transfer: The nature of the N-bands of porphyrins and chlorophylls revealed through CAM-B3LYP, CASPT2, and SAC-CI calculations. *J. Phys. Chem. B*, 2006, **110**(31), 15624–15632.

76. Sponer, H. and Teller, E. Electronic spectra of polyatomic molecules. *Rev. Mod. Phys.*, 1941, **13**(2), 75.

77. Longuet-Higgins, H. C. Some recent developments in the theory of molecular energy levels. *Adv. Spectrosc.*, 1961, **2**, 429–472.

78. Ballhausen, C. J. and Hansen, A. E. Electronic spectra. *Annu. Rev. Phys. Chem.*, 1972, **23**, 15–38.

79. Azumi, T. and Matsuzaki, K. What does the term "vibronic coupling" mean? *Photochem. Photobiol.*, 1977, **25**(3), 315–326.

80. Lax, M. The Franck–Condon principle and its application to crystals. *J. Chem. Phys.*, 1952, **20**, 1752.

81. Markham, J. J. Interaction of normal modes with electron traps. *Rev. Mod. Phys.*, 1959, **31**(4), 956–989.

82. McCumber, D. E. Theory of vibrational structure in optical spectra of impurities in solids. I. Singlets. *J. Math. Phys.*, 1964, **5**(2), 221–230.

83. Holstein, T. Studies of polaron motion: Part I. The molecular-crystal model. *Ann. Phys.*, 1959, **8**(3), 325342.

84. Dexter, D. L. A theory of sensitized luminescence in solids. *J. Chem. Phys.*, 1953, **21**(5), 836–850.

85. Reimers, J. R. A practical method for the use of curvilinear coordinates in calculations of normal-mode-projected displacements and Duschinsky rotation matrices for large molecules. *J. Chem. Phys.*, 2001, **115**, 9103–9109.

86. Frisch, M. J., Trucks, G. W., Schlegel, H. B., Scuseria, G. E., Robb, M. A., Cheeseman, J. R. et al. *Gaussian 16, Revision C.01*. Gaussian Inc., Wallingford CT, 2016.

87. Wales, D. J. A microscopic basis for the global appearance of energy landscapes. *Science*, 2001, **293**, 2067–2070.

88. Saunders, P. T. *An Introduction to Catastrophe Theory*. Cambridge University Press, 1980.

89. Reimers, J. R., McKemmish, L. K., McKenzie, R. H. and Hush, N. S. Non-adiabatic effects in thermochemistry, spectroscopy and kinetics: the general importance of all three Born–Oppenheimer breakdown corrections. *Phys. Chem. Chem. Phys.*, 2015, **17**(38), 24641–24665.

90. Born, M. and Oppenheimer, R. Zur Quantentheorie der Molekeln. *Ann. Phys.*, 1927, **389**, 457–484.

91. Hush, N. S. Adiabatic rate processes at electrodes. I. Energy-charge relationships. *J. Chem. Phys.*, 1958, **28**(5), 962–972.

92. Levich, V. G. and Dogonadze, R. R. Theory of rediationless electron transitions between ions in solution. *Dokl. Akad. Nauk SSSR Ser. Fiz. Khim.*, 1959, **124**, 123–126.

93. Levich, V. G. and Dogonadze, R. R. Adiabatic theory for electron-transfer processes in solution. *Dokl. Akad. Nauk SSSR.*, 1960, **133**, 158–161.

94. Frank-Kamenetskiĭ, M. D. and Lukashin, A. V. Electron-vibrational interactions in polyatomic molecules. *Sov. Phys. Usp.*, 1975, **18**(6), 391–409.

95. Reimers, J. R. and Watts, R. O. The structure and vibrational spectra of small clusters of water molecules. *Chem. Phys.*, 1984, **85**(1), 83–112.

96. Wilson, E. B., Decius, J. G., Cross, P. G. and Lagemann, R. T. Molecular vibrations. *Am. J. Phys.*, 1955, **23**.

97. Reimers, J. R., and Watts, R. O. A local mode potential function for the water molecule. *Mol. Phys.*, 1984, **52**(2), 357–381.

98. Condon, E. U. Nuclear motions associated with electron transitions in diatomic molecules. *Phys. Rev.*, 1928, **32**(6), 858–872.

99. Herzberg, G. and Teller, E. Schwingungsstruktur der Elektronenübergänge bei mehratomigen Molekülen. *Z. Phys. Chem.*, 1933, **21B**, 410–446.

100. Small, G. J. Herzberg–Teller vibronic coupling and the Duschinsky effect. *J. Chem. Phys.*, 1971, **54**(8), 3300–3306.

101. Chappell, P. J. and Ross, I. G. Vibronic coupling by out-of-plane modes in pyridine, pyrazine and quinoxaline. *Chem. Phys. Lett.*, 1976, **43**, 440–445.

102. Albrecht, A. C. "Forbidden" character in allowed electronic transitions. *J. Chem. Phys.*, 1960, **33**, 156–169.

103. Ziegler, L. and Albrecht, A. C. Vibronic calculations in benzene by CNDO/S. *J. Chem. Phys.*, 1974, **60**, 3558–3561.

104. Craig, D. P. and Small, G. J. Totally symmetric vibronic perturbations and the phenanthrene 3400Å spectrum. *J. Chem. Phys.*, 1969, **50**, 3827–3834.

105. Piepho, S. B., Krausz, E. R. and Schatz, P. N. Vibronic coupling model for calculation of mixed valence absorption profiles. *J. Am. Chem. Soc.*, 1978, **100**, 2996–3005.

106. Chappell, P. J., Fischer, G., Reimers, J. R. and Ross, I. G. Electronic spectrum of 1,5-naphthyridine: theoretical treatment of vibronic coupling. *J. Mol. Spectrosc.*, 1981, **87**(2), 316–330.

107. Fisher, G. *Vibronic Coupling*. Academic Press, London, 1984.

108. London, F. Zur Theorie nicht adiabatisch verlaufender chemischer Prozesse. *Z. Phys.*, 1932, **74**, 143174.

109. Shuler, K. E. Adiabatic correlation rules for reactions involving polyatomic intermediate complexes and their application to the formation of OH ($^2\sum$+) in the H_2 - O_2 flame. *J. Chem. Phys.*, 1953, **21**(4), 624–632.

110. Ross, I. G. Vibrational electronic coupling and a closer look at a severe case. *Isr. J. Chem.*, 1975, **14**, 118–123.

111. Piepho, S. B., Krausz, E. R. and Schatz, P. N. Vibronic coupling model for calculation of mixed valence absorption profiles. *J. Am. Chem. Soc*., 1978, **100**, 2996–3005.

112. Piepho, S. B. and Schatz, P. N. *Group Theory in Spectroscopy: with Applications to Magnetic Circular Dichroism*. Wiley, New York, NY, 1983.

113. Holstein, T. Studies of polaron motion: Part II. The "small" polaron. *Ann. Phys*., 1959, **8**, 343–389.

114. Hush, N. S. Inequivalent XPS binding energies in symmetrical delocalized mixed-valence complexes. *Chem. Phys*., 1975, **10**, 361–366.

115. Öpik, U. and Pryce, M. H. L. Studies of the Jahn-Teller effect. I. A survey of the static problem. *Proc. Math. Phys. Eng. Sci*.,1957, **238**(1215), 425–447.

116. Pekar, S. and Deigen, M. Quantum states and optical transitions of electron in a polaron and at a color center of a crystal. *Zh. Eksp. Teor. Fiz*., 1948, **18**(6), 481–486.

117. Rätsep, M., Pajusalu, M. and Freiberg, A. Wavelength-dependent electron-phonon coupling in impurity glasses. *Chem. Phys. Lett*. 2009, **479**(1), 140–143.

118. Ingold, C. K. and Leeke, F. M. Electronic spectra of polyatomic molecules. Vibrations of the $^1B_{2u}$ state of benzene. *Nature*, 1946, **157**, 46–47.

119. Azumi, T. and Matsuzaki, K. What does the term vibronic coupling mean? *Photochem. Photobiol*., 1977, **25**, 315–326.

120. Ballhausen, C. J. and Hansen, A. E. Electronic spectra. *Annu. Rev. Phys. Chem.*, 1972, **23**, 15–38.

121. Freiberg, A., Rätsep, M., Timpmann, K. and Trinkunas, G. Excitonic polarons in quasi-one-dimensional LH1 and LH2 bacteriochlorophyll *a* antenna aggregates from photosynthetic bacteria: A wavelength-dependent selective spectroscopy study. *Chem. Phys*., 2009, **357**(1), 102–112.

122. Rätsep, M., Linnanto, J. M., Muru, R., Biczysko, M., Reimers, J. R. and Freiberg, A. Absorption-emission symmetry breaking and the different origins of vibrational structures of the ^1Q_y and ^1Q_x electronic transitions of pheophytin *a*. *J. Chem. Phys*., 2019, **151**, 165102.

123. Zazubovich, V., Tibe, I. and Small, G. J. Bacteriochlorophyll *a* Frank-Condon factors for the S0-S1(Q_y) transition. *J. Phys. Chem. B*, 2001, **105**(49), 12410–12417.

124. Reimers, J. R., Rätsep, M. and Freiberg, A. Asymmetry in the Q_y fluorescence and absorption spectra of chlorophyll *a* pertaining to exciton dynamics. *Frontiers in Chemistry*, 2020, **8,** 588289.

125. Rätsep, M., Linnanto, J. and Freiberg, A. Mirror symmetry and vibrational structure in optical spectra of chlorophyll *a*. *J. Chem. Phys*., 2009, **130**(19), 194501.

126. McKemmish, L. K., McKenzie, R. H., Hush, N. S. and Reimers, J. R. Quantum entanglement between electronic and vibrational degrees of freedom in molecules. *J. Chem. Phys*., 2011, **135**(24), 244110.

127. McKemmish, L., McKenzie, R. H., Hush, N. S. and Reimers, J. R. Electron-vibration entanglement in the Born–Oppenheimer description of chemical reactions and spectroscopy. *Phys. Chem. Chem. Phys*., 2015, **17**(38), 24666–24682.

128. Reimers, J. R. and Hush, N. S. Electron transfer and energy transfer through bridged systems. I. Formalism. *Chem. Phys*., 1989, **134**(2–3), 323–354.

129. Shi, Y., Liu, J.-Y. and Han, K.-L. Investigation of the internal conversion time of the chlorophyll *a* from S$_3$, S$_2$ to S$_1$. *Chem. Phys. Lett.*, 2005, **410**, 260–263.

130. Paschenko, V. Z., Gorokhov, V. V., Korvatovskiy, B. N., Bocharov, E. A., Knox, P. P., Sarkisov, O. M. et al. The rate of Q$_x$→Q$_y$ relaxation in bacteriochlorophylls of reaction centers from *Rhodobacter sphaeroides* determined by kinetics of the ultrafast carotenoid bandshift. *Biochim. Biophys. Acta Bioenerg.*, 2012, **1817**, 1399–1406.

131. Visser, H. M., Somsen, O. J. G., van Mourik, F., Lin, S., van Stokkum, I. H. M. and van Grondelle, R. Direct observation of sub-picosecond equilibration of excitation energy in the light-harvesting antenna of *Rhodospirillum rubrum*. *Biophys. J*., 1995, **69**, 1083–1099.

132. Ganago, A. O., Parker, E. P., Laible, P. D., Albrecht, A. C. and Owens, T. G. Femtosecond dynamics of population and coherence of the S$_2$ singlet excited state of bacteriochlorophyll (the Q$_x$ absorption band) in vivo and in vitro. *Laser Phys*., 1995, **5**, 693–698.

133. Causgrove, T. P., Yang, S. and Struve, W. S. Polarized pump-probe spectroscopy of exciton transport in bacteriochlorophyll *a*-protein from *Prosthecochloris aestuarii*. *J. Phys. Chem*., 1988, **92**, 6790–6795.

134. Chai, J.-D. and Head-Gordon, M. Long-range corrected hybrid density functionals with damped atom-atom dispersion corrections. *Phys. Chem. Chem. Phys*., 2008, **10**(44), 6615–6620.

135. Sirohiwal, A., Berraud-Pache, R., Neese, F., Izsák, R. and Pantazis, D. A. Accurate computation of the absorption spectrum of chlorophyll *a* with pair natural orbital coupled cluster methods. *J. Phys. Chem. B*, 2020, **124**(40), 8761–8771.

136. Santoro, F., Lami, A., Improta, R. and Barone, V. Effective method to compute vibrationally resolved optical spectra of large molecules at finite temperature in the gas phase and in solution. *J. Chem. Phys*., 2007, **126**(18), 184102.

137. Santoro, F., Lami, A., Improta, R., Bloino, J. and Barone, V. Effective method for the computation of optical spectra of large molecules at finite temperature including the Duschinsky and Herzberg–Teller effect: The *Q*x band of porphyrin as a case study. *J. Chem. Phys*., 2008, **128**(22), 224311.

138. Cerezo, J., Aranda, D., Avila Ferrer, F. J., Prampolini, G. and Santoro, F. Adiabatic-molecular dynamics generalized vertical Hessian approach: A mixed quantum classical method to compute electronic spectra of flexible molecules in the condensed phase. *J. Chem. Theory Comput*., 2020, **16**(2), 1215–1231.

139. Santoro, F. and Jacquemin, D. Going beyond the vertical approximation with time-dependent density functional theory. *WIREs Comput. Mol. Sci*., 2016, **6**(5), 460–486.

140. Götze, J. P., Anders, F., Petry, S., Witte, J. F. and Lokstein, H. Spectral characterization of the main pigments in the plant photosynthetic apparatus by theory and experiment. *Chem. Phys.*, 2022, **559**, 111517.

141. Kundu, S., Roy, P. P., Fleming, G. R. and Makri, N. Franck–Condon and Herzberg–Teller signatures in molecular absorption and emission spectra. *J. Phys. Chem. B*, 2022, **126**(15), 2899–2911.

142. Rätsep, M., Pajusalu, M., Linnanto, J. M. and Freiberg, A. Subtle spectral effects accompanying the assembly of bacteriochlorophylls into cyclic light harvesting complexes revealed by high-resolution fluorescence spectroscopy. *J. Chem. Phys.*, 2014, **141**(15), 155102.

143. Pajusalu, M., Rätsep, M., Trinkunas, G. and Freiberg, A. Davydov splitting of excitons in cyclic bacteriochlorophyll *a* nanoaggregates of bacterial light-harvesting complexes between 4.5 and 263 K. *ChemPhysChem.*, 2011, **12**(3), 634–644.

144. Freiberg, A., Pajusalu, M. and Rätsep, M. Excitons in intact cells of photosynthetic bacteria. *J. Phys. Chem. B*, 2013, **117**, 11007–11014.

145. Freiberg, A., Rätsep, M. and Timpmann, K. A comparative spectroscopic and kinetic study of photoexcitations in detergent-isolated and membrane-embedded LH2 light-harvesting complexes. *Biochem. Biophys. Acta*, 2012, **1817**(8), 1471–1482.

146. Sundström, V., Pullerits, T. and van Grondelle, R. Photosynthetic light-harvesting: Reconciling dynamics and structure of purple bacterial LH2 reveals function of photosynthetic unit. *J. Phys. Chem. B*, 1999, **103**(13), 2327–2346.

147. Hu, X., Ritz, T., Damjanović, A., Autenrieth, F. and Schulten, K. Photosynthetic apparatus of purple bacteria. *Q. Rev. Biophys.*, 2002, **35**(1), 1–62.

148. Hunter, C. N., Daldal, F., Thurnauer, M. C. and Beatty, J. T. (eds). *The Purple Phototrophic Bacteria*. Springer, Dordrecht, 2009.

149. Green, B. R. and Parson, W. W. (eds). *Ligh-Harvesting Antennas in Photosynthesis*. Kluwer Academic Publishers, Dordrecht-Boston-London, 2003.

150. Osad'ko, I. S. Theory of light absorption and emission by organic impurity centers. In *Spectroscopy and Excitation Dynamics of Condensed Molecular Systems* (Agranovich, V. M. and Hochstrasser, R. M., eds). North–Holland, Amsterdam, 1983, 438–514.

151. Wu, H.-M., Rätsep, M., Lee, I.-J., Cogdell, R. J. and Small, G. J. Exciton level structure and energy disorder of the B850 ring of the LH2 antenna complex. *J. Phys. Chem. B*, 1997, **101**(38), 7654–7663.

152. Freiberg, A., Timpmann, K., Ruus, R. and Woodbury, N. W. Disordered exciton analysis of linear and nonlinear absorption spectra of antenna bacteriochlorophyll aggregates: LH2-only mutant chromatophores of *Rhodobacter sphaeroides* at 8 K under spectrally selective excitation. *J. Phys. Chem. B*, 1999, **103**(45), 10032–10041.

153. Hochstrasser, R. M. and Whiteman, J. D. Exciton band structure and properties of a real linear chain in a molecular crystal. *J. Chem. Phys.*, 1972, **56**, 5945–5958.

154. Hanson, D. M. Effect of the exciton bandwidth on electron-phonon coupling in molecular crystals. *Chem. Phys. Lett.*, 1976, **43**, 217–220.

155. Kell, A., Khmelnitskiy, A., Jassas, M. and Jankowiak, R. Dichotomous disorder versus excitonic splitting of the B800 band of *Allochromatium vinosum*. *J. Phys. Chem. Lett.*, 2018, **9**(14), 4125–4129.

156. Ostrowski, W. Michael S. Tswett–inventor of column chromatography. *Folia Biol.*, 1968, **16**(4), 429–448.

157. Craig, D. P. The Franck–Condon principle and the size of the excited benzene molecule. *J. Chem. Soc.*, 1950, 2146–2151.

158. Craig, D. P. The role of E_g^+ vibrations in the 2600-A benzene band system. *J. Chem. Soc.*, 1950, 59–62.

159. Cai, Z.-L., Crossley, M. J., Reimers, J. R., Kobayashi, R. and Amos, R. D. Density-functional theory for charge-transfer: the nature of the N-bands of porphyrins and chlorophylls revealed through CAM-B3LYP, CASPT2, and SAC-CI calculations. *J. Phys. Chem. B*, 2006, **110**(31), 15624–15632.

160. Reimers, J. R. and Hush, N. S. A unified description of the electrochemical, charge distribution, and spectroscopic properties of the special-pair radical cation in bacterial photosynthesis. *J. Am. Chem. Soc.*, 2004, **126**, 4132–4144.

Klorofülli spektroskoopia: põhimõtted, kaasaegne kõrglahutusel põhinev käsitlus ja eelseisvad väljakutsed

Jeffrey R. Reimers, Margus Rätsep, Juha Matti Linnanto ja Arvi Freiberg

Ülevaates käsitletakse ideid ja põhimõtteid, mis aitavad mõista klorofüllide omadusi ning funktsioneerimist nii gaasifaasis, lahustes kui ka valk-maatriksites e pigment-valgu kompleksides. Me näitame, kuidas nende printsiipide sihipärane rakendamine klorofüll-a, bakterklorofüll-a ja feofütiin-a kõrglahutusega mõõdetud spektrite interpreteerimisel, sümbioosis kõrgetasemeliste kvantkeemiliste arvutustega, annab unikaalset teavet fotosünteesi alusprotsesside kohta. Pöörates erilist tähelepanu nn Duschinsky rotatsioonile ja mitte-adiabaatilisele interaktsioonile, aga ka keskkonna omaduste ja temperatuuri mõjule klorofülli spektritele, tuvastasime klorofülli kiirgus- ja neeldumisspektrite kriitilise asümmeetrilisuse. Duschinsky rotatsiooni tulemusena kiirgavad klorofüllid valgust neeldumise suhtes erineval energial, samas kui mitte-adiabaatilisus põhjustab valguse polarisatsiooni muutumist. Selle avastuse mõju klorofülli funktsiooni mõtestamisele fotosünteesis võib olla suur, sest varasemad mudelid valdavalt eeldasid neeldumise ja kiirguse sümmeetrilisust.